Universidad Nacional Autónoma de México
POSGRADO EN CIENCIAS FÍSICAS
INSTITUTO DE CIENCIAS FÍSICAS

CO-ACCELERATION OF PARTICLES AND SURFACE PLASMONS IN NANOSTRUCTURES.

TESIS
QUE PARA OPTAR POR EL GRADO DE:
MAESTRA EN CIENCIAS (FÍSICA)

PRESENTA:
MERLYN JAQUELINE JUÁREZ GUTIÉRREZ

TUTOR PRINCIPAL
DR. WOLF LUIS MOCHÁN BACKAL
INSTITUTO DE CIENCIAS FÍSICAS, UNAM.

MIEMBROS DEL COMITÉ TUTOR

DR. THOMAS WERNER STEGMANN,
INSTITUTO DE CIENCIAS FÍSICAS, UNAM.

DR. RAUL PATRICIO ESQUIVEL SIRVENT
INSTITUTO DE FÍSICA, UNAM.

CIUDAD UNIVERSITARIA, CD. MX., JUNIO 2023

Agradecimientos

Agradezco a CONACYT por mi beca de maestría.

A Luis Mochán, por todo su apoyo, supervisión, enseñanza y disposición para todas las discusiones a lo largo de mis estudios.

A RM, a quien no puedo expresar con palabras cuánto agradezco por su apoyo y compañía.

Agradezco a PAPIIT que financia al proyecto *Óptica lineal, no lineal y coherente en sistemas atómicos, moleculares y nanoestructurados* con clave IN109822, del cual recibí una beca para la obtención del grado de Maestra en Ciencias Físicas.

Acknowledgments

I acknowledge the support of CONACYT through a scholarship.

I am grateful to Luis Mochán for his support, supervision, teaching and willingness to all our discussions through my studies.

Words cannot express how grateful I am to RM for all his support and company.

I acknowledge PAPIIT, which funds the project *Linear, non-linear and coherent optics in atomic, molecular and nanostructured systems* with grant IN109822, under which I received a scholarship to obtain a Master's Degree in Physical Sciences.

RESUMEN

La aceleración de partículas cargadas es de interés tanto por el mero conocimiento de los aspectos físicos involucrados como por las múltiples aplicaciones que puede ofrecer. Dichas aplicaciones van desde investigación en ciencia básica a herramientas de seguridad. Las partículas aceleradas en los actuales aceleradores convecionales alcanzan energías de TeV, pero éstos son incapaces de mantener campos eléctricos superiores a 40 megavolts por metro, por lo que requieren grandes instalaciones y consumos de energía. Esto resulta muy costoso y limita la utilidad de los aceleradores. Lo anterior nos ha motivado a buscar soluciones alternativas, tales como el desarrollo de aceleradores compactos y de bajo presupuesto.

En esta tesis estudiamos la aceleración de partículas cargadas debida a su interacción con plasmones de superficie (PS). Proponemos una configuración metal-vacío-metal que forma un canal a lo largo de cuyo eje se aceleran las partículas. Usando la relación de dispersión del PS del sistema, modulamos su velocidad de fase para incrementar la interacción efectiva entre las partículas cargadas y el campo del PS. Para acelerar al PS, las interfaces metálicas que forman el canal son gradualmente separadas. Resolvemos la ecuación del potencial del PS en el régimen no retardado asumiendo que los cambios de la geometría a lo largo de la cavidad son muy suaves, por lo que los cambios en el vector de onda local son lentos comparados con otras distancias relevantes. De esta manera, podemos tratar al sistema como traslacionalmente invariante localmente y usar la relación de dispersión del canal homogéneo. Sintonizando la aceleración del SP con la de una partícula nominal de tal manera que mantengan una fase relativa constante, en analogía a una surfeadora montando una ola, obtuvimos la expresión analítica de la anchura requerida del canal como una función de la posición a lo largo del canal. Mostramos que el diseño es longitudinalmente estable y que las partículas que difieren en sus condiciones iniciales de las de la partícula nominal también son aceleradas a lo largo del canal, pero, oscilando alrededor de ésta.

Estudiamos la excitación del PS con luz, iluminando un acoplador de rejilla. Asumiendo que el patrón sobre la superficie es de ángulo bajo, obtenemos una expresión analítica perturbativa del campo del PS. Situamos la rejilla en la apertura por la que las partículas emergen del canal. A medida que se excita el PS, su energía viaja hacia la región de aceleración del canal pero su fase viaja en dirección a su salida. Del análisis perturbativo derivamos el coeficiente de acoplamiento entre el campo del PS y el campo de la fuente de excitación. Conociendo la aceleración a la que una partícula está sujeta en el canal, podemos calcular su ganancia de energía en una cierta distancia recorrida. Así, proponemos un valor de ganancia de energía y calculamos las longitudes requeridas para alcanzarla. Como nuestro análisis es únicamente válido en la aproximación no retardada, las energías están restringidas a valores no relativistas.

Asumiendo un metal plasmónico típico para la cavidad, energías más pequeñas pero del orden de la masa en reposo de la partícula acelerada y el campo fuente de un láser pulsado típico resonante con el PS, las dimensiones del canal resultaron ser del orden de nanómetros en la dirección transversal y de centímetros en la longitudinal, lo cual conlleva a ciertas dificultades técnicas. Estas distancias son funciones simples del inverso de la frecuencia del PS y de la amplitud del campo

eléctrico incidente. Discutimos regímenes alternativos, materiales y estrategias de excitación para hacer factible el acelerador plasmónico propuesto.

ABSTRACT

The acceleration of charged particles is of interest both for the mere knowledge of the physical aspects involved and for the multiple applications it can offer. Such applications range from basic scientific research to security tools. Particles accelerated in current conventional accelerators reach energies of TeV, but they are incapable of maintaining electric fields greater than 40 megavolts per meter, so they require large facilities and energy consumption. Their expense limits the usefulness of accelerators. This has motivated us to search alternative solutions, such as the development of compact and low-budget accelerators.

In this thesis, we study the acceleration of charged particles due to their interaction with the electric field associated with surface plasmons (SP). We propose a channel-like metal-vacuum-metal configuration to accelerate particles along the axis of the cavity. Using the dispersion relation of the SP we modulate its phase velocity taking advantage of its dependence on the geometrical parameters of the cavity to increase the effective interaction between the SP and injected particles. To accelerate the SP, we gradually separate the metal interfaces that make up the channel. Laplace's equation for the SP potential in the non-retarded regime is solved assuming very gentle changes in the geometry along the cavity, so that the changes in the local wavevector of the SP are negligible in the lengthscale of other relevant physical quantities. Thus, we can treat the system as locally translationally invariant and use the dispersion relation of a locally homogeneous cavity. Tuning the acceleration of the SP to that of a nominal accelerated particle so that the particle remains at a region of constant phase, in analogy to a surfer riding a wave, we obtained analytical expressions for the required width of the cavity as a function of position along the axis. We show that the design is longitudinally stable and that particles with initial conditions that differ substantially from those of the nominal particle are also accelerated along the channel, with some oscillations around the nominal position.

We study the excitation of the SP through light coupled by a grating. Assuming a low-angle grating, we perturbatively obtain analytical expressions for the SP field. The grating is situated at the exit opening of the accelerating channel. As the SP is excited its energy travels towards the accelerating region of the channel but its phase travels towards the exit. From the perturbative analysis, we derived analytically the coupling coefficient relating the accelerating SP's electric field to that of the source. Once we know the acceleration to which a particle in the channel is subjected, we compute the energy gain for a given distance traveled. Thus, we propose a desired output energy and we calculate the length of the cavity required to achieve it. In our analysis, we used a non-retarded approximation for the field. Thus, our current analysis is constrained to the non-relativistic regime.

Assuming a typical plasmonic metal for the cavity, an energy smaller but of the order of the rest mass of the accelerated particle and the source field of a typical pulsed laser resonant with the SP, the width of the channel turned out to be of the order of nanometers and its length of the order of centimeters, which gives rise to some technical difficulties. These distances are given by simple functions of the inverse of the SP frequency and the amplitude of the incoming electric

field. We discuss alternative regimes, materials, and excitation strategies to make our proposed plasmonic accelerator feasible.

CONTENTS

LIST OF FIGURES

Chapter 1

INTRODUCTION

1.1. Background and Perspectives on Accelerators

The acceleration of charged particles has had an important role for society. High-quality charged particle bunches have many applications in medicine, basic science research and technology. Regarding basic science, ultra-fast electron diffraction has allowed the determination of the structure of matter in equilibrium such as the shape of molecules, proteins, complex assemblies such as viruses. It is also the basis for the emerging field of atomically resolved dynamics which requires high quality, high energy electron beams to determine the structural dynamics of matter [1, 2, 3]. Some of the most widely used applications in medicine are radiation therapy for the treatment of cancer and the production of x-rays for imaging of tissues [4].

Nowadays, the accelerated particles may reach energies of the order of TeV's in colliders such as the *Large Hadron Collider, (LHC)* and other linear colliders (LC) [5], as can be seen in the Livingston chart, Fig. 1.1, that shows that every decade there has been an energy increase of about one and a half orders of magnitude.

These so-called *conventional accelerators* have technical and physical limitations. For example, they have a limited energy gradient due to limits on the accelerating fields, and thus, they require kilometer-scale facilities to reach highly relativistic beams. These facilities have very high building and maintenance costs. Their extensive infrastructure requires experimenters to travel large distances and to hire highly qualified persons to conduct the experiments. These aspects make them exclusive machines, while many industrial and medical applications await accelerators to become accessible with reduced costs and sizes.

The actual needs and difficulties related to particle acceleration [7] have motivated the search for novel alternatives to develop accessible accelerators, such as table top GeV accelerators, as research tools. These are some of our main objectives.

At present, there are several compact accelerator proposals. They include the Dielectric Laser Accelerators (DLA) based on the general principle of periodic electric field reversal structures [8], and accelerators based on them such as DLA's integrated with photonic circuits [9]. Others use narrow band THz pulses in a scheme based on cascading dielectric-lined wave-guides, [10]. An older proposal and one of the most explored ones is the laser plasma acceleration termed as *Wakefield Acceleration*, by Tajima and Dawson in 1979 [11]. It is based on the use of fields associated with excited charge density oscillations within a plasma and uses laser technology instead of radio-frequency fields. A laser is fired into the plasma *sweeping* electrons out of its way, leaving positively charged ions along the center of its path. These charged regions make a *wakefield* that originates oscillations of the charge density named *bulk plasmons* whose associated electric fields can reach hundreds of GV/m, thousands of times bigger than those currently achieved by conventional accelerators [12, 13]. Nevertheless, this kind of plasma-laser accelerators have other difficulties that have not yet been overcome. For example, they are subject to three main mechanisms that limit the energy gain of the accelerated particles. These are laser diffraction, phase shifts between

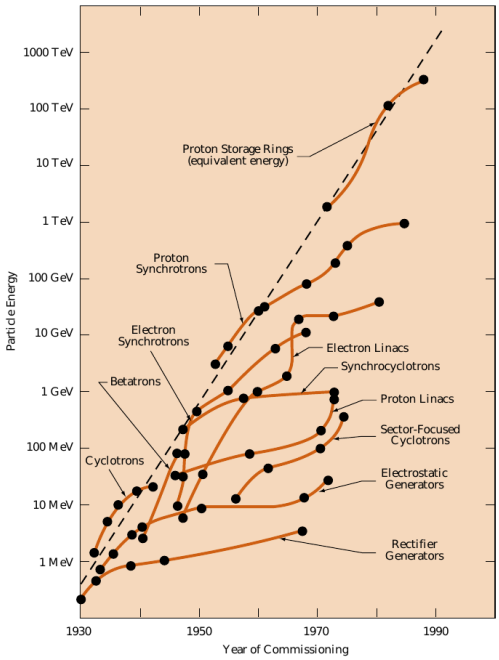

Figure 1.1: Energy of particle beams produced by accelerators in the target's frame as a function of time. This graph is called a Livingston chart after M. Stanley Livingston, the physicist who conceived it in the 1960's [6].

the particles being accelerated and the accelerating fields, laser energy losses when exciting the plasma waves and large angular dispersions of the beam, [13, 14, 15]. Motivated by the research on *Wakefield Acceleration*, which relies on longitudinal electric fields associated to bulk charge density oscillations, in this thesis we propose and study the feasability of using charge density oscillations at surfaces, i.e., *surfaces plasmons* as an alternative to laser plasma particle acceleration schemes.

1.2. A bold proposal: Surface Wave based Accelerators.

Surface plasmons, (SP's) are electromagnetic modes of metallic-dielectric interfaces whose field decays evanescently along the direction perpendicular to the interfaces. SP's have already found many potential applications and may find more soon by exploiting their electromagnetic field confinement in sub-wavelength scales. There are applications such as bio-sensing [16], nano-imaging, and super-lensing [17, 18], among others. There is also much interest in enhancing the electric field through the coupling of light sources to SP's, which has brought to mind its possible application to accelerate charged particles near the interface. In my bachelor's degree project [19] I studied the interaction of charged particles with the electric field of SP's. I also studied the amplification of an optical incident field coupled to the SP through a dielectric prism using the Kretschmann configuration [20] and through a grating diffraction [21]. I explored the dynamics of a charged particle interacting with the perpendicular component of the electric field that accelerates the particle away from the surface. The displacement of the particle is due to the perpendicular inhomogeneity of the field, which gives rise to a *ponderomotive force* proportional and opposite in direction to the gradient of the squared electric field. Researchers have explored this acceleration during the last two decades and reported some experimental results. For example, energy gains of 0.4keV and 2keV for accelerated electrons using the ponderomotive effect of a high gradient electromagnetic field associated with SP excited with a laser with intensities of TW/cm^2 and GW/cm^2 have been

reported [22, 23].

Our question is, is it possible to accelerate charged particles continually and efficiently using the parallel electric field associated with SP's? Henceforth, we study the properties and tunability of the phase velocity of SP's via gradual changes in the material structure in which they are excited. Accelerating SP's may allow them to sync with the motion of a charged particle near the interface along which the SP's propagate and accelerate them synchronously. For this purpose, we derive the dispersion relation of SP's propagating along the interface between vacuum and planar media structures, and we analize their dependence on geometrical parameters.

We worked out a mechanism to persistently accelerate a charged particle centered in a channel. The channel is made of two separated semi-infinite metals whose flat interfaces are placed one in front of the other. To mantain the particles in the midpoint, we use the ponderomotive effect associated with the SP's field from each interface, which give rise to a force that points away from the surfaces and a null transverse force right in the middle. To overcome the asynchrony between particles and the SP mode, we sought mechanisms that would allow us to change the phase velocity of SP. We initially explored different surface modes on various structures and media to find suitable candidates for this task, such as dielectric-dielectric and metallodielectric superlattices, to search their surface modes. We studied *Tamm waves* [24], surface waves that propagate along the interface between a homogeneous dielectric medium and a periodic dielectric-dielectric superlattice. We studied these waves because the energy dissipation is less in dielectric than in metallic structures. We obtained their dispersion relation through the poles of the optical reflection amplitude, which lies outside the light-cone in vacuum. However, their phase velocity is always high, as their dispersion relation lies within the light cones of one of the dielectrics that make up the superlattice. This result limits the range of modulation of their phase velocity and, consequently, that of the particles. Then, we studied surface modes on a periodic metallodielectric superlattice consisting of two films, a dielectric and a metallic one, repeated periodically. Using effective medium theory, we obtained the effective dielectric function of the periodic medium, with different values along two different directions of the system, namely, one along the plane parallel to the layers and along the perpendicular direction to the layers. The effective medium resulted anisotropic, and the isofrequencies of the dispersion relation of its electromagnetic modes are ellipses, instead of circles as in isotropic media. Nevertheless, if one value of the principal dielectric functions is negative, the curves in the wavevector space of the dispersion relation become hyperbolas. For this reason, these superlattices are known as *hyperbolic metamaterials*. The superficial waves at the interface between the superlattice and the space seemed good candidates. Since their phase velocities are not high and their dispersion relation depends on the thickness of each film, their velocities can be modulated through an extensive range of values in the wave vector space. We can modulate the phase velocity by changing the filling fraction of the layers through a gradient of the width of the films. To study the *Tamm waves* we used a *transfer matrix* formalism. And for the metallodielectric supperlattice we used the *effective media approximation*, and the propagation of electromagnetic waves in anisotropic media.

In the end we didn't use the surface modes described above, and they are not fundamental in developing the mechanism on which we did focus, but they were part of our preliminary studies and they helped me to understand the relevant criteria for the design of our proposal. The details of these approaches are offered in the appendix B, where the *transfer matrix* and *effective media approximation* formalisms are presented in detail, and they are used to derive the response function of the lattices. As metallodielectric lattices result in anisotropic effective media, the propagation of light in anisotropic media is also presented.

Lastly, we settled on analyzing the co-acceleration of particles and SP's using two semi-infinite metals separated by a variable distance between their interfaces. In this metal-insulator-metal (MIM) arrangement, the dependence of the SP dispersion relation on the separation between interfaces allows us to accelerate the surface plasmon mode in step with a judiciously chosen nominal charged particle. The acceleration of SP's allows us to accelerate charged particles steadily along the space between interfaces, which forms a channel. We found an analytical function

describing how the interfaces should separate for the SP's to keep in phase with the motion of the nominal particle. We used the expression for the separation to obtain the explicit position dependent wavevector and the amplitude and phase of the electric field. Then, we calculated the trajectories that particles with different initial conditions would follow once immersed in the electric field of the SP to test the stability of our acceleration scheme. Finally, we propose a mechanism to excite the SP using a grating coupler consisting of sinusoidal rough surfaces of low angle situated at the exit of the accelerating channel. We performed a perturbative analysis up to first order on the roughness height and obtained the coupling coefficient between an incident electromagnetic field with the SP. Thus, we computed the energy gained by particles in terms of the incident field.

It is worth mentioning that others have also investigated the acceleration of particles along the propagation direction of a SP in the last couple of years. The proposal is to excite a SP in a square grating structure and to modify the effective index of refraction by changing the geometrical parameters of the grating, such as its period and height, to accelerate the SP, achieving electron energies of $\approx$ 19keV [25]. We learnt about this result after we started our calculations. It is comforting that others believe the co-acceleration of particles and surface plasmons is a viable mechanism to accelerate particles.

This work has the following structure. In the following two chapters (Chs. 2 and 3) we present the electromagnetic theory of metals and the theory of surface plasmons. Then, in Ch. 4 we develop our new proposal, followed by the results (Ch. 5) and their analysis. We finish with our conclusions and outlook (Ch. 6). Additionally, we present appendices A and B) with details of some cumbersome calculations and of the work done during my research that didn't end up being fundamental to our results, as mentioned above, but that we believe that can be valuable for interested students and researchers, and with detailed developments which may be useful to some readers.

Chapter 2

ELECTRODYNAMICS OF METALS

In this chapter we present the main classical model that describes the reponse of metals to applied electromagnetic fields. We start presenting the Maxwell equations which describe the spatial and temporal dependence of the electromagnetic fields within material media. Then we describe the collective oscillations of the charge density within conductors, the *bulk plasmons* or simply *plasmons*. Finally, we derive the dielectric function of conducting media using the *Drude Model*. We finish with a brief discussion of the Drude response within different frequency ranges.

2.1. Maxwell Equations

The description of the electromagnetic response of media is governed by Maxwell equations, which describe the spatial and temporal dependence of the electromagnetic fields in an arbitrary media in terms of the displacement $\boldsymbol{D}$ and the magnetic $\boldsymbol{H}$ fields, and relate them to the electric field $\boldsymbol{E}$ field and the magnetic flux density $\boldsymbol{B}$. For the description of fields within media the total current density $\boldsymbol{j} = \boldsymbol{j}_i + \boldsymbol{j}_{\text{ext}}$ is written as the sum of an internal $\boldsymbol{j}_i$ and an external $\boldsymbol{j}_{\text{ext}}$ contribution, with a corresponding separation for the charge density $\rho = \rho_i + \rho_{\text{ext}}$. The external sources *drive* the system while the internal $(\rho_i, \boldsymbol{j}_i)$ react to the external stimulus and are incorporated in the displacement field and magnetic fields $\boldsymbol{D}$ and $\boldsymbol{H}$ [26].

The *macroscopic* electromagnetic equations in media are

$$\nabla \cdot \boldsymbol{D} = 4\pi\rho_{\text{ext}}, \tag{2.1a}$$

$$\nabla \cdot \boldsymbol{B} = 0, \tag{2.1b}$$

$$\nabla \times \boldsymbol{E} = -\frac{1}{c}\frac{\partial \boldsymbol{B}}{\partial t}, \tag{2.1c}$$

$$\nabla \times \boldsymbol{H} = \frac{4\pi}{c}\boldsymbol{j}_{\text{ext}} + \frac{1}{c}\frac{\partial \boldsymbol{D}}{\partial t}. \tag{2.1d}$$

The internal sources are described by the polarization $\boldsymbol{P}$ and magnetization $\boldsymbol{M}$, related to $\boldsymbol{D}$ and $\boldsymbol{H}$ through

$$\boldsymbol{D} = \boldsymbol{E} + 4\pi\boldsymbol{P}, \tag{2.2a}$$

$$\boldsymbol{H} = \boldsymbol{B} - 4\pi\boldsymbol{M}. \tag{2.2b}$$

$\boldsymbol{P}$ is related to the internal charge density through

$$\nabla \cdot \boldsymbol{P} = -\rho_i, \tag{2.3}$$

and is usually interpreted as the electric dipolar moment per unit volume caused by the motion of the electrons and ions within the material. Substituting Eqs. (2.3) and (2.2a) in Gauss law, Eq.

(2.1a), we obtain

$$\begin{aligned} \nabla \cdot (\boldsymbol{E} + 4\pi \boldsymbol{P}) =& \nabla \cdot \boldsymbol{E} + 4\pi \nabla \cdot \boldsymbol{P} = 4\pi \rho_{\text{ext}}, \\ \nabla \cdot \boldsymbol{E} =& 4\pi(\rho_{\text{ext}} + \rho_i), \end{aligned} \tag{2.4}$$

so that the source of the macroscopic electric field includes all contributions to the charge density.

The magnetization $\boldsymbol{M}$ is related to the internal current density through

$$\boldsymbol{j}_i = c\nabla \times \boldsymbol{M} + \frac{\partial}{\partial t}\boldsymbol{P}, \tag{2.5}$$

so it is related to the contributions beyond the motion of the charges that give rise to the polarization, and it is usually interpreted as the magnetic moment per unit volume.

In magnetostatics, Ampère's law yields a relation between the flux density $\boldsymbol{B}$ and the total current,

$$\begin{aligned} \nabla \times \boldsymbol{H} =& \frac{4\pi}{c}\boldsymbol{j}_{\text{ext}} \\ \nabla \times (\boldsymbol{B} - 4\pi \boldsymbol{M}) =& \frac{4\pi}{c}\boldsymbol{j}_{\text{ext}} \\ \nabla \times \boldsymbol{B} =& \frac{4\pi}{c}\left(\boldsymbol{j}_{\text{ext}} + \boldsymbol{j}_i\right), \end{aligned} \tag{2.6}$$

showing that the sources of $\boldsymbol{B}$ include all the contributions to the electric current. A similar conclusion may be derived from the Ampère-Maxwell law.

As we are interested in the optical properties of materials and specifically of metals, we will study the response to applied electromagnetic fields. Limiting ourselves to small electric and magnetic fields magnitudes, the dependences of $\boldsymbol{D}$ on $\boldsymbol{E}$ and of $\boldsymbol{H}$ on $\boldsymbol{B}$ are approximately linear and are given by

$$\boldsymbol{D} = \epsilon \boldsymbol{E}, \tag{2.7}$$

$$\boldsymbol{H} = \frac{1}{\mu}\boldsymbol{B}, \tag{2.8}$$

where ϵ is called the **permittivity** and μ the **permeability** of the media. The simplest case corresponds to that in which the reponse functions ϵ and μ are constants, but in general they depend on position, frequency, and in the nonlinear case, they may also depend on the field strength. Henceforth, ϵ also receives the name of *dielectric function*.

2.1.1. Charge Density Oscilations in Conductors

The principal characteristic of conductors is the presence of free electrons that can move within the bulk. The typical model of conductors is a regular arrangement of atoms immersed in a *gas* of free electrons. Each atom contributes with a few of its electrons to the gas and these can move all around the conductor, which is why they are called shared electrons.

The fundamental oscillation of the charge density in conductors is called *plasmon*. Plasmons can be well described and its frequency can be obtained using a classical model of free electron as a gas. Let's consider a region in a conductor where the charge density is perturbed. As the mass of ions is 3 orders of magnitude bigger than the electronic mass, $m_i \sim 10^3 m_e$, they can be considered static in comparison to electrons. The motion of electrons away from some region, might produce a positive charge that attracts them back. Due to their inertia, as they return, they can overrun the equilibrium condition creating an accumulation of negative charge, which will produce repulsive forces that will push the electrons away, leaving behind a positively charged region. This coming and going would repeat until its associated energy is dissipated. These charge oscillations are called *plasma oscillations* and have a characteristic frequency ω_p, the plasma frequency.

Consider an electron gas with an equilibrium number density of charge carriers n moving freely on a positively charged background and interacting with the electromagnetic field. Each electron is accelerated by the electric field according to Newton's second law, $m_e d^2\mathbf{r}/dt^2 = -e\mathbf{E}$, where m_e, e are the electronic mass and charge, respectively. Their motion creates a current density, $\boldsymbol{j} = -ned\boldsymbol{r}/dt$, with derivative $\partial\boldsymbol{j}/\partial t = -ned^2\boldsymbol{r}/dt^2$. Let's get rid of the acceleration in terms of the force, obtaining $\partial\mathbf{j}/\partial t = (ne^2/m_e)\mathbf{E}$. Integrating over a large surface S that completely encloses the charged region

$$\frac{d}{dt}\left(\int_S d\boldsymbol{a}\cdot\boldsymbol{j}\right) = \frac{ne^2}{m_e}\int_S d\boldsymbol{a}\cdot\mathbf{E}. \tag{2.9}$$

Using Gauss law and the continuity equation in their integral form, we obtain the equation that describes the oscillation of the charge within S,

$$\frac{d^2Q}{dt^2} = -\frac{4\pi ne^2}{m_e}Q, \tag{2.10}$$

whose solution is $Q(t) = Q(0)e^{-i\omega_p t}$, where the plasma frequency ω_p is equal to

$$\omega_p = \sqrt{\frac{4\pi ne^2}{m_e}}. \tag{2.11}$$

This derivation of the plasma oscillations was taken from Ref. [27]. The plasma frequency of a metal is much larger than that of thermal oscillations, hence their quantization is important when describing the electronic dynamics of solids. This quantized plasma oscillation is the *plasmon*, and has energies in the range of $\mathcal{E}_p = \hbar\omega_p \sim 5 - 15eV$ for noble metals [28].

2.2. Drude Model of Metals

Over a wide range of frequencies, the optical properties of metals can be explained by the *Drude Model*, which successfully describes characteristics of metals such as the conductivity and resistance in terms of the equilibrium electronic density and other parameters of the free electron gas, modelling the conduction charges as a gas of electrons that move against a fixed background of positive ion cores, and assuming that the main interactions are just collisions between electrons with ions and that the electromagnetic field does not vary over distances comparable to the free electron path.[1]

The Drude model considers the motion of electrons under the influence of an electric field $\boldsymbol{E}$ determined by the Lorentz force $\boldsymbol{F} = -e\boldsymbol{E}$ and a friction force $\boldsymbol{F}_f = -\Gamma d\boldsymbol{r}/dt$ resulting from collisions, where Γ is a constant. The equation of motion is

$$m\frac{d^2\boldsymbol{r}}{dt^2} + \Gamma\frac{d\boldsymbol{r}}{dt} = -e\boldsymbol{E}. \tag{2.12}$$

For a time-harmonic driving field, $\boldsymbol{E} = \boldsymbol{E}_0 e^{-i\omega t}$, the non-transient solution is

$$\boldsymbol{r} = \frac{e/m}{\omega^2 + i\omega\nu}\boldsymbol{E}, \tag{2.13}$$

where $\nu = \Gamma/m$ is the collision frequency. The displaced electrons contribute to the macroscopic polarization through their dipole moment, $\boldsymbol{p} = -e\boldsymbol{r}$ which, considering a number density of n electrons per unit volume, yields a polarization $\boldsymbol{P} = -ne\boldsymbol{p}$. Since the displacement vector is given

[1] More details about the assumptions and quantities obtained from the Drude model and its refinements can be found in standard solid state books [29]. Here we confine ourselves to its most basic features, as required for our work.

by Eq. (2.2a), equating it with Eq. (2.7) yields $\boldsymbol{D} = \boldsymbol{E} + 4\pi\boldsymbol{P} = \epsilon\boldsymbol{E}$. Substituting the polarization above we solve for the permittivity

$$\epsilon(\omega) = \left(1 - \frac{\omega_p^2}{\omega^2 + i\omega\nu}\right), \tag{2.14}$$

where $\omega_p^2 = 4\pi ne^2/m$ is the *Drude plasma frequency*, as previously obtained in Eq.(2.11). In general, Gauss law implies that collective charge oscillations may only exist for frequencies for which $\epsilon(\omega) = 0$. In the Drude model, ω_p satisfies this condition, but not in more sophisticated models that also include contributions to the permittivity from bound electrons.

The dielectric function from the Drude model may be split into real and imaginary parts

$$\epsilon(\omega) = \epsilon'(\omega) + i\epsilon''(\omega), \tag{2.15}$$

where

$$\epsilon'(\omega) = 1 - \frac{\omega_p^2\tau^2}{1 + \omega^2\tau^2}, \tag{2.16a}$$

and

$$\epsilon''(\omega) = \frac{\omega_p^2\tau}{\omega(1 + \omega^2\tau^2)}. \tag{2.16b}$$

Here, $\tau = 1/\nu$ is the relaxation time, which at room temperatures is typically of the order of $10^{-14}s$.

Applying an electromagnetic field or another perturbing agent to bring the charges out of equilibrium, creates currents inside conducting media. The current density is related to the conductivity σ through *Ohm's law*, $\boldsymbol{j}_i = \sigma\boldsymbol{E}$. An ideal conductor has infinite conductivity $\sigma = \infty$, but real metals have finite conductivity due to collisions of the electrons with each other and with the ion lattice, and at finite frequencies, due to the electronic inertia.

The relation between the dielectric function and the conductivity can be obtained by identifying $\boldsymbol{P} = (\epsilon - 1)\boldsymbol{E}/4\pi$, using the law of conservation of charge, $\boldsymbol{\nabla} \cdot \boldsymbol{j}_i = -\partial\rho_i/\partial t$, and replacing the charge density by $\boldsymbol{\nabla} \cdot P = -\rho_i$, which give us $\boldsymbol{j}_i = \partial\boldsymbol{P}/\partial t = -i\omega\boldsymbol{P}$, and $\frac{-i\omega(\epsilon-1)}{4\pi}\boldsymbol{E} = \sigma\boldsymbol{E}$, from which

$$\epsilon = 1 + 4\pi i\frac{\sigma}{\omega}. \tag{2.17}$$

In the description of the electromagnetic response of metals, ϵ is usually used only for the response of bound charges that leads to the polarization, while σ is used to describe the contribution of free charges to the curren flow. However, at optical frequencies, it is more convenient to treat both contributions on a similar footing as done above, including the contributions of the motion of all internal charges in ϵ and equivalently, in σ.

The imaginary part of the permittivity ϵ'' determines the amount of absortion of light inside the medium, which from Eq. (2.17) is related to the real part of the conductivity σ' [28].

2.2.1. Discussion of the Drude Response

Given its simplicity, it is remarkable that the Drude model of metals has been so successful. Some of its original premises, such as postulating a mean free path of the order of the interatomic distance and an average electronic speed of the order of a thermal speed are wrong. The mean free path is much larger, as collisions are with defects, impurities and phonons, but the speed is much larger, as the electrons in a conductor form a degenerate electron gas. Both effects compensate each other [29].

It is insightful to study the dielectric function for a variety of different frequency regimes with respect to the collision frequency ν and the plasma frequency ω_p [28]. Assuming $\nu \ll \omega_p$, for frequencies close the plasma frequency $\omega \approx \omega_p$, there is a small damping and $\epsilon(\omega)$ is almost real,

$$\epsilon(\omega) \approx 1 - \frac{\omega_p^2}{\omega^2}. \tag{2.18}$$

Hence, electromagnetic waves have a small dissipation. However, they do not propagate within metals if $\omega < \omega_p$ as $\epsilon < 0$. For very low frequencies, $\omega \ll \nu$ the imaginary part of the dielectric function is larger than the real part, $\epsilon'' > |\epsilon'|$, and it diverges when $\omega \to 0$ as $\epsilon''(\omega) \approx 4\pi\sigma(0)/\omega$ [30].

Despite the success of Drude's free-electron describing metals, it is known that the theory fails in the visible and near-ultraviolet regions as it doesn't take into account interband transitions. For example, in silver (Ag) the actual plasma frequency, for which $\epsilon'(\omega) = 0$, is found to be smaller than that predicted by the free electron model [31], shifting from around 9 eV to the neighborhood of 3.8 eV. The reason is that the onset of transitions from a fairly flat d band to the conduction sp band pulls the real part of the dielectric function above its Drude value. In some metals there may be an overlap between the actual plasma frequency and the frequency of interband transitions, leading to absorption and damping of the plasmon excitation. This is not the case for Ag, whose plasmon is quite well defined.

Chapter 3

SURFACE PLASMONS

Surface plasmons are charge oscillations that propagate along interfaces between dielectric and conductive media with associated electromagnetic waves evanescently confined along the direction perpendicular to the interface, as illustrated in Fig. 3.1.

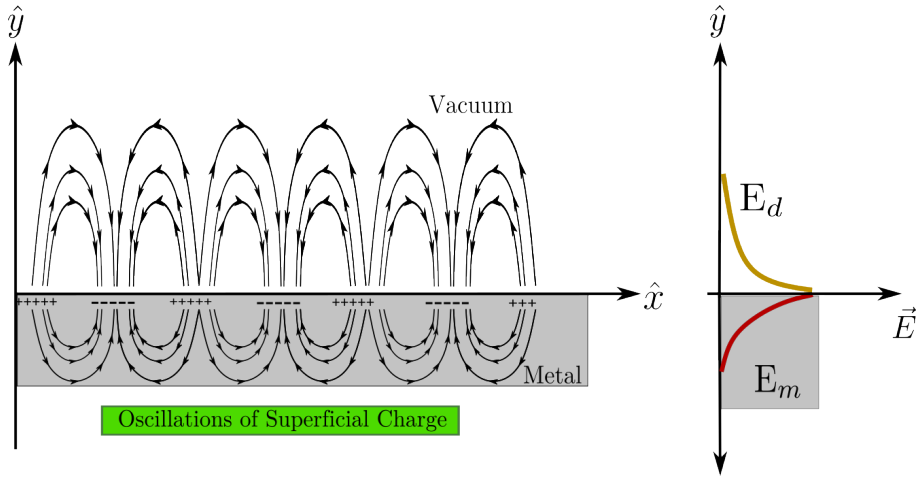

Figure 3.1: Surface plasmons are charge oscillations at surfaces with electromagnetic fields evanescently confined to the neighborhood of the interface between dielectric and conductive media. Some surface charges and the field lines they produce are schematically illustrated, as well as the dependence of the magnitude of the evanescent field on position above (E_v) and below (E_m) the interface.

We begin this chapter with some historical background regarding research on SP's. Then we describe the theory of SP propagation and their properties; solving Maxwell equations we obtain their fields and dispersion relation. Then we study the SP's characteristic distances: their penetration length, wavelength and their propagation length. Lastly, we describe in detail the ponderomotive force, a force that a charged particle inmersed in the SP's field feels, and which is due to the perpendicular exponential decay of the field.

3.1. Background

Around the '50s a big amount of experimental and theoretical work on the topic of charge oscillations in conductors, specifically in thin films, was done. The experimental work on the energy loss of electron beams impinging at metallic thin films, guided the hypotheses and the research

on collective charge oscillations. In 1956, David Pines discussed and theoretically described the observations of discrete energy losses, which led him to the idea of quantized collective oscillations of conduction electrons, and in analogy with earlier work on plasma oscillations in gas discharges, he called them *plasmons* [32]. A year later, Rufus Ritchie also studied electron energy losses in thin films and showed that plasmon modes can exist near the surface of metals. He developed the first theoretical description of surface plasmons [33]. This was verified experimentally two years later by Powell and Swan [34]. These and later works built the current basis for the research on the excitation of plasmons. For example, important contributions on the excitation of surface plasmons were proposed in the works of Andreas Otto [35], Enrich Kretschmann and Heinz Raether [36], who developed easily implemented and accesible methods for excitation of SP's in thin metallic films.

From then on till the present times, the research of SP's in metals, semiconductors, and 2D materials with many morphologies, different structures and sizes, has allowed the understanding of optical properties of nano particles of different metals, nonlinear effects, etc. [33]. The current research in SP's is very active due to progress in the fabrication of nanostructures. This has allowed some control on the propagation of the SP's, making them available for many applications such as data storage, miniature solar cells and biosensors. Among others, one of the most explored is the concentration and channeling of energy using subwavelength structures [37]. Work is also being carried out on the excitation efficiency of SP's in different structures with different kinds of light that the progress in laser technology has brought. An example of this research was done by J.M. Villarreal who studied the fields of SP's excited by short pulses of light obtaining the intensity of the SP fields as a function of the pulse duration [38]. Besides, different methods for SP excitation have been devised. The methods of Otto and Kretschmann consist of increasing the wave vector of the incident light beyond the light cone of vacuum, in order to couple it directly to the SP. They used a dielectric material with dielectric constant larger than that of vacuum in the proximity of the metallic interface. Other coupling mechanisms include increasing the wave vector through diffraction, adding to the relatively small optical wave vector a reciprocal lattice vector [39] of a grating or a rough surface, or employing the near field produced by isolated nanostructures above or near the metal surface such as metallic nanoparticles, or holes and sharp edges in the metallic films, or arrays of those [40, 41].

3.2. Frequency of the Surface Plasmon

A simple estimate of the frequency on the surface charge oscillations can be done as for the bulk plasmons (Sec. 2.1.1) but restricting the region where charge can flow to a semiinfinite space bounded by the interface, i.e. half of the field lines corresponding to surface charges lie outside of the conductor region and don't affect the motion of the free charges. Henceforth, the equation of motion for the charge at the interface and enclosed within some surface S is

$$\frac{d^2Q}{dt^2} = -\frac{4\pi ne^2}{2m_e}Q = \frac{\omega_p^2}{2}Q, \tag{3.1}$$

instead of Eq. (2.10). Its solution $Q(t) = Q_0 e^{-i\omega_{\mathrm{SP}}t}$ oscillates with the resonance frequency

$$\omega_{\mathrm{SP}} = \omega_p/\sqrt{2} \tag{3.2}$$

that differs from that of the bulk plasmons ω_p by a constant factor [27].

3.3. Propagation of Surface Plasmons: Dispersion Relation

Now we study the properties of SP's by solving Maxwell equations in two media, conductive and dielectric, separated by a flat interface on which boundary conditions are applied, as illustrated in

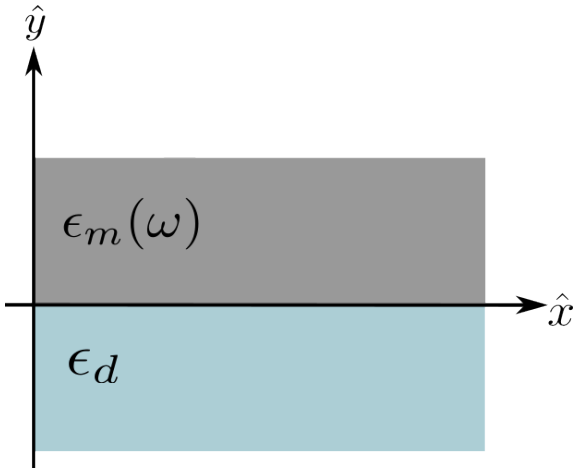

Figure 3.2: Flat interface between dielectric and conductive media with corresponding permittivities ϵ_d and $\epsilon_m(\omega)$.

Fig. 3.2. We assume the SP propagates along $\hat{x}$ and decays along $\hat{y}$ as we move away from the interface. Translational symmetry in time and along the surface allows us to consider an oscillatory dependence on t and x, so we replace ∂_t by $-i\omega$ and ∂_x by iQ in the field equations, where ω is the frequency and $\boldsymbol{Q} = (Q, 0, 0)$ the wavevector along the surface, which is the same in both media.

Let's assume the dielectric has a real dielectric constant ϵ_d and occupies the inferior half-space and the conductor with a dielectric function $\epsilon_m(\omega)$ occupies the superior half-space, as shown in Fig. 3.2. We consider electromagnetic waves with p polarization described by the fields $\boldsymbol{E} = (E_x, E_y, 0)$ and $\boldsymbol{H} = (0, 0, H_z)$. Maxwell equations within the α-th medium (α=m,d) yield

$$\begin{aligned} E_y(z) &= \frac{Q}{q\epsilon_\alpha} H_z(y), \\ E_x(y) &= i\frac{1}{q\epsilon_\alpha}\frac{\partial}{\partial y} H_z(y), \\ \frac{\partial^2}{\partial y^2} H_z(y) &- \left(\epsilon_\alpha q^2 - Q^2\right) H_z(y) = 0, \end{aligned} \tag{3.3}$$

where we've introduced the wavenumber in vacuum $q = \omega/c$. The solutions are waves confined to the surface with exponential decay along the $\hat{y}$ direction, perpendicular to the interface. Within the conductor, $y > 0$, the solution is

$$\begin{aligned} H_z^+(y) &= H^+ e^{i(Qx-\omega t)} e^{-k_m y}, \\ E_x^+(y) &= -i\frac{k_m}{q\epsilon_m} H^+ e^{i(Qx-\omega t)} e^{-k_m y}, \\ E_y^+(y) &= \frac{Q}{q\epsilon_m} H^+ e^{i(Qx-\omega t)} e^{-k_m y}, \end{aligned} \tag{3.4}$$

within the conductor, $y > 0$. The fields within the dielectric $y < 0$ are

$$\begin{aligned} H_z^-(y) &= H^- e^{i(Qx-\omega t)} e^{k_d y}, \\ E_x^-(y) &= i\frac{k_d}{q\epsilon_d} H^- e^{i(Qx-\omega t)} e^{k_d y}, \\ E_y^-(y) &= \frac{Q}{q\epsilon_d} H^- e^{i(Qx-\omega t)} e^{k_d y}. \end{aligned} \tag{3.5}$$

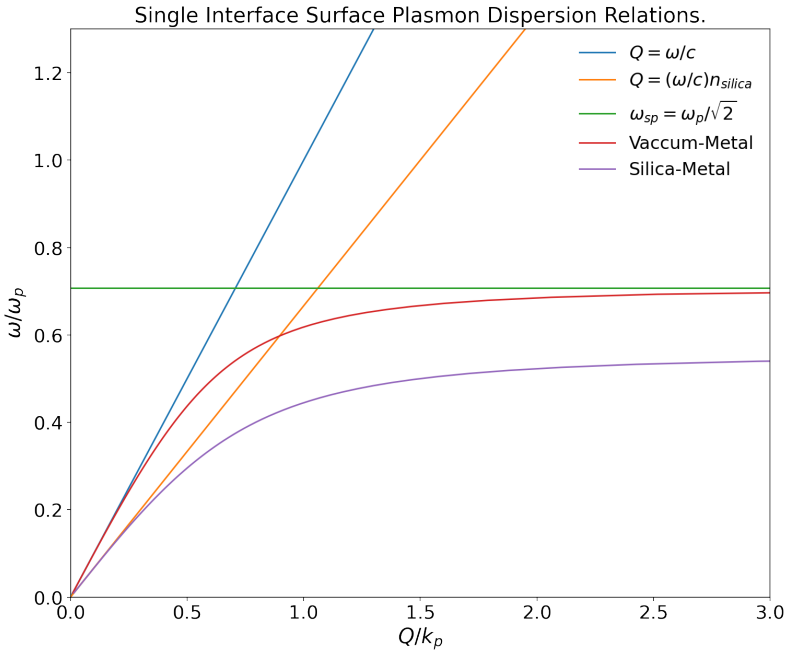

Figure 3.3: Dispersion relation ω vs Q of surface plasmons propagating along the interface between a Drude metal without damping and vacuum, and the interface between metal and Silica. The projected light cones of vacuum and of Silica are also shown as well as the asymptotic surface plasmon frequency given by Eq. (3.2). The frequency is normalized to the plasma frequency ω_p and the wavevector to $k_p = \omega_p/c$ (Taken from *Plasmonics*, by Stefan A. Maier [28].)

Here, k_m and k_d are the penetration constants in each media, $E^{\pm}$ and $H^{\pm}$ are the amplitudes of electric and magnetic fields where the signs indicate the $y > 0$ and the $y < 0$ half spaces respectively and $\pm ik_\alpha$ is the normal component of the wavevector in medium α, obtained from the corresponding wave equation (3.3),

$$\begin{aligned} k_m^2 &= Q^2 - \epsilon_m q^2, \\ k_d^2 &= Q^2 - \epsilon_d q^2. \end{aligned} \tag{3.6}$$

The continuity of the projections of the electric field and magnetic fields parallel to the interface $y = 0$, $E_x^+(0) = E_x^-(0)$ and $H_z^+(0) = H_z^-(0)$, leads to two equations for the amplitudes $H^{\pm}$ which have a finite solution only if

$$\frac{k_m}{k_d} = -\frac{\epsilon_m}{\epsilon_d}. \tag{3.7}$$

Substituting Eqs. (3.6), we get the dispersion relation of the surface plasmons

$$Q = q\sqrt{\frac{\epsilon_d \epsilon_m}{\epsilon_d + \epsilon_m}}. \tag{3.8}$$

Fig. 3.3 shows typical dispersion curves corresponding to a metal with a Drude dielectric function without damping next to vacuum $\epsilon_v = 1$ and next to Silica $\epsilon_{SiO_2} = 2.25$. It also shows the projection of the light cones of vacuum and of Silica upon the interface and the asymptotic SP frequency given by Eq. (3.2). It can be observed that the SP wave vector on each interface lies outside their corresponding dielectric light cone. Hence, one realizes that SP's can't be directly excited via a beam of light incident from vacuum and that it is necessary to provide the photons

with additional momentum to excite SP's. The additional momentum can be given with the aforementioned techniques, either coupling light to SP's using prisms or via diffraction with a grating to match the momentum along the surface. For example, the curves show that when the light passes through a dielectric media like Silica with $\epsilon > 1$ the excitation of the SP on a nearby metal-vacuum interface might be achieved since the wave vector Q may take values between ω/c and $\sqrt{\epsilon_{\mathrm{SiO_2}}}\omega/c$ for appropriate angles of incidence.

We also observe the asymptotic behavior of the SP, which shows that for large values of Q the group and phase velocities go to zero, so the perturbation does not propagate.

Surface plasmons with s polarization don't exist for nonmagnetic materials. This result is easily derived in the same way as for the p polarized case, as shown in detail in [28].

3.3.1. Characteristic Lengths

In planar metallodielectric geometries the solution of Maxwell equations yield the retarded dispersion relation Eq. (3.8) and the electric fields associated to the surface plasmons which are a mix of transverse and longitudinal components with respect to the propagation direction, and which decay as $|y| \to \infty$. We rewrite the electric fields given in Eqs. (3.4) and (3.5) as

$$\boldsymbol{E}_\alpha(x, y, t) = \boldsymbol{E}_{\alpha 0} e^{i(Qx-\omega t)\pm k_\alpha y}, \tag{3.9}$$

where the wavevector $\boldsymbol{Q} = (Q, 0, 0)$ determines the propagation, k_α the penetration constant within medium α, and the sign before $\pm k_\alpha$ the decay direction.

Parallel wavelength and propagation length

For a real metal whose dielectric function is complex ($\epsilon_m = \epsilon'_m + i\epsilon''_m$), the parallel component of the wavevector is a complex quantity $Q = Q' + iQ''$ as well. The real part of Q determines the plasmon wavelength $\lambda_{\mathrm{SP}} = 2\pi/Q'$, and the imaginary part is related to the decay $e^{-Q''x}$ of the SP as it propagates, so the propagation length of the plasmon is given by

$$L_{\mathrm{SP}} = \frac{1}{Q''}. \tag{3.10}$$

Assuming a real value of ω and that $\mathrm{Im}(\epsilon_m) \ll |\mathrm{Re}(\epsilon_m)|$, the SP's dispersion relation, Eq. (3.8), can be written as [39]

$$Q \approx q\left[\left(\frac{\epsilon'_m\epsilon_d}{\epsilon'_m+\epsilon_d}\right)^{1/2} + i\frac{\epsilon''_m}{2(\epsilon'_m)^2}\left(\frac{\epsilon'_m\epsilon_d}{\epsilon'_m+\epsilon_d}\right)^{3/2}\right]. \tag{3.11}$$

Notice that propagation of the SP is possible only for $\epsilon'_m < 0$ and $|\epsilon'_m| > \epsilon_d$, which may be fulfilled in metals or in doped semiconductors at low enough frequencies.

For example, the Drude plasmon frequency of Ag is around $\hbar\omega_p \approx 8.9$ eV, ($\omega_p = 13$ PHz) and for a collision time $\tau = 18$ fs and visible radiation $\lambda = 600$ nm, the real and imaginary values of the Drude dielectric function are, $\mathrm{Re}(\epsilon_{\mathrm{Ag}})(0.24\omega_p) = -16$, $\mathrm{Im}(\epsilon_{\mathrm{Ag}})(0.24\omega_p) = 0.30$, so the propagation length would be equal to $L_{\mathrm{SP}} = 150\,\mu$m. Recall though that a realistic model of Ag would have to incorporate the contributions of bound electrons to the dielectric response.

Perpendicular penetration depth

Substituting Eq. (3.8) in Eq. (3.6) for each media we obtain the penetration constants

$$\begin{aligned} k_m &= \sqrt{q^2\frac{\epsilon_m\epsilon_d}{\epsilon_d+\epsilon_m} - \epsilon_m q^2}, \\ &= q\sqrt{-\frac{\epsilon_m^2}{\epsilon_m+\epsilon_d}}, \end{aligned} \tag{3.12a}$$

$$k_d = \sqrt{q^2 \frac{\epsilon_m \epsilon_d}{\epsilon_d + \epsilon_m} - \epsilon_d q^2}, \\ = q\sqrt{-\frac{\epsilon_d^2}{\epsilon_m + \epsilon_d}}. \tag{3.12b}$$

From Eq. (3.8), for the SP's to exist we require $\epsilon_d < -\epsilon_m$, so that k_α in Eqs. (3.12a) and (3.12b) are real numbers, which correspond to exponential decay of the field along $\hat{y}$. Since the amplitude decreases exponentially as $e^{-k_\alpha |y|}$ normally to the vacuum-metal interface, the distance from the surface where the field has fallen to $1/e$, known as the penetration depth, is given by

$$\delta_\alpha = \frac{1}{k_\alpha}. \tag{3.13}$$

Substituting Eqs. (3.12a) and (3.12b), we obtain

$$\delta_m = \left| \frac{\lambda}{2\pi} \frac{\sqrt{\epsilon_m + \epsilon_d}}{\epsilon_m} \right|, \tag{3.14a}$$

$$\delta_d = \left| \frac{\lambda}{2\pi} \frac{\sqrt{\epsilon_m + \epsilon_d}}{\epsilon_d} \right|, \tag{3.14b}$$

with λ the free space wavelength. For a Drude metal with parameters corresponding to Ag and visible light with $\lambda = 600$ nm, the penetration depths in the metal and in vacuum are $\delta_m = 23\,\mu$m and $\delta_d = 370\,\mu$m respectively, which are one order of magnitude smaller and of the same order as wavelength in vacuum respectively.

In the non-retarded limit the free space wavelength is much greater than other relevant length-scales, so from Eq. (3.6) one gets

$$k_\alpha \approx Q, \tag{3.15}$$

i.e., the penetration depth is $1/Q$, 2π times smaller than the SP wavelength λ_{SP}.

3.3.2. Ponderomotive Effect

One of the most characteristic features of the SP propagation is the evanescent decay away from the interface, which gives an inhomogeneous character to its electromagnetic field.

The gradient of the electromagnetic field amplitude gives rise to a *ponderomotive force*. This force, discovered by Kelvin (1845) [42], is a physical phenomenon that an electrically charged body experiences in the presence of an electric fields with oscillatory and inhomogeneous nature. It causes the charged body to move towards regions with a weaker field strength. This effect is non-linear and is one of the principles of the *plasma wakefield* acceleration, mentioned before.

In the quasistatic limit we can neglect magnetic effects, and since the ponderomotive effect happens to be perpendicular we restrict our analysis to the motion along the normal coordinate, y. Let's consider a particle immersed in the electric field of the SP just above the vacuum metal interface, given by Eq. (3.9). Its equation of motion along the $\hat{y}$ direction is

$$m\frac{d^2}{dt^2}y = qE_y = q\left(\frac{E_0 e^{i(Qx-\omega t)-k_v y} + c.c}{2}\right), \tag{3.16}$$

where *c.c.* is the complex conjugated of the field, q is the electric charge of the particle and k_v the penetration constant in vacuum. Notice that the variable y appears on both sides of the equation. We separate the position y into slow and fast contributions, $y = y_s + y_f$, due to the oscillations and inhomogeneity of the field, as shown in Fig. 3.4 where on average the displacement of the particle in one cycle is not null because the field changes in space, i.e., the forces that pushes a particle away from the surface is smaller than the force that pulls it back half a cycle later, when

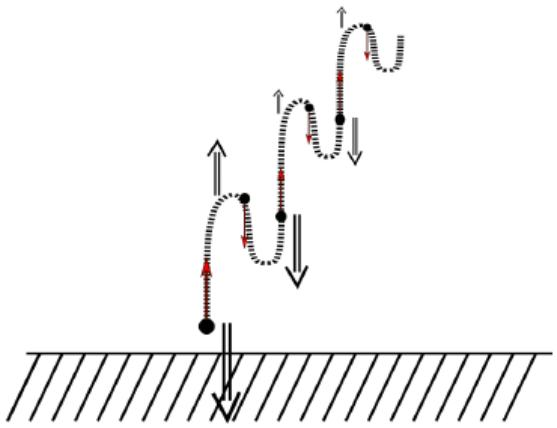

Figure 3.4: Schematic path of a charged particle along the direction perpendicular to the SP propagation. The path is a consequence of the spatial inhomogeneity of the SP field. The thicker arrows illustrate the field direction and strength and the thin red arrows illustrates the force on a negative particle. The average displacement in a cycle is not null, unlike the case for an oscillatory homogeneous electromagnetic field. The motion parallel to the surface is introduced only to facilitate visualization.

the particle is farther away, as indicated with different sized arrows in the figure. The analysis below is carried out for a constant value of the parallel coordinate x.

Suppose the fast motion in a single cycle has a small amplitude compared to the penetration depth, so that a Taylor expansion of the field around the position given by the slow coordinate can be done. As the force depends on the field evaluated at the actual position y occupied by the particle, the equation of motion is

$$\begin{aligned} m(\ddot{y}_s + \ddot{y}_f) =& \frac{q}{2}\left(E_y(x, y_s, t) + c.c\right) + \frac{qy_f}{2}\partial_y\left(E_y(x, y_s, t) + c.c\right), \\ =& \frac{q}{2}\left(E_0 e^{i(Qx-\omega t)-k_v y_s} + c.c\right) + \frac{qy_f}{2}\partial_y\left(E_0 e^{i(Qx-\omega t)-k_v y_s} + c.c\right) \end{aligned} \tag{3.17}$$

that can be separated by size contributions, as $\ddot{y_s} \ll \ddot{y_f}$ though y_f is considered tiny.

The fast coordinate obeys

$$\begin{aligned} m\ddot{y}_f =& \frac{q}{2}\left(E_0 e^{i(Qx-\omega t)-k_v y_s} + c.c\right), \\ =& \frac{q}{2}\left(E_0 e^{i(Qx-\omega t)-k_v s y_s} + c.c\right), \end{aligned} \tag{3.18}$$

which yields a harmonic oscillatory solution for times so short that y_s may be considered constant,

$$y_f = -\left(\frac{q}{2m\omega^2}\right)\left(E_0 e^{i(Qx-\omega t)-k_v y_s} + c.c\right). \tag{3.19}$$

The equation for the slow coordinate is given by the second part of Eq. (3.17),

$$\begin{aligned} m\ddot{y}_s =& \left(\frac{qy_f}{2}\right)\partial_y\left(E_0 e^{i(Qx-\omega t)-k_v y_s} + c.c\right), \\ =& -\left(\frac{qy_f k_v}{2}\right)\left(E_0 e^{i(Qx-\omega t)-k_v y_s} + c.c\right). \end{aligned} \tag{3.20}$$

Substituting Eq. (3.19), we obtain

$$\begin{aligned} m\ddot{y}_s &= \left(\frac{q^2 k_v}{m\omega^2}\right)\left(\frac{E_0 e^{i(Qx+\omega t)} + c.c}{2}\right)^2 e^{-2k_v y_s}, \\ &= \left(\frac{q^2 k_v}{4m\omega^2}\right)\left[(E_0 e^{i(Qx+\omega t)})^2 + (E_0^* e^{-i(Qx+\omega t)})^2 + 2|E_0|^2\right] e^{-2k_v y_s}, \end{aligned} \tag{3.21}$$

which contains fast terms that oscillate with a frequency 2ω which average to zero displacement and which we ignore. The force that produces the displacement along the perpendicular direction of the particle, is then given just by

$$F_p = m\ddot{y}_s = \left(\frac{q^2 k_v}{4m\omega^2}\right)|E_0|^2 e^{-2k_v y_s}, \tag{3.22}$$

termed as the *ponderomotive force*. F_p can be rewritten in terms of the gradient of the field as

$$F_p = -\left(\frac{q^2}{8m\omega^2}\right)\nabla\left(|\boldsymbol{E}|^2\right), \tag{3.23}$$

which explicits that it points towards the direction along which the field decreases, pushing away particles from the interface.

This perpendicular force has a meaningful effect in the dynamics of charged particle near the surface where the SP propagates. For example there are works where this force was used to accelerate particles away from the surface, that in combination with the pararallel component of the force, yields trayectories of particles that are not straight lines [22, 23].

Chapter 4

PARTICLE ACCELERATION BY SURFACE PLASMONS

Surface plasmon based electron acceleration has been a topic of research in the last few decades. As mentioned in Sec. 1.2, many works have been reported and some experiments have been carried out with promising results. This chapter is devoted to the development of the theoretical foundations and results of the calculations made to justify the feasibility of what we previously called *a bold proposal*.

Building on the previous results for SP propagation on single metallic interfaces, we study the eigenmodes for two metallic surfaces separated a given distance in the subwavelength scale, each one in front of the other such that they set up a kind of channel. Then, we calculate the dynamics of a charged particle in the middle of the channel, halfway between the interfaces. As we aim to accelerate a particle parallel to the SP's propagation, we envisaged that this configuration will allow the cancellation of the ponderomotive force effect upon the charged particles, and they might remain stable around the middle of the channel while being steadily accelerated.

This chapter starts by computing the solution for the electrostatic potential of the system composed of two parallel flat metallic plate's interfaces and the dispersion relation of the two eigenmodes of the system, which depend on the plate's separation, a geometric parameter that characterizes the arrangement of the plates. Since the SP's electric field is oscillatory, no net acceleration would be experienced by charged particles along the axis of the channel. The particles would spend some of their time in regions where the field accelerates them and the rest in regions where it slows them down. Henceforth, a question arises, how to accelerate charged particles constantly along the channel's axis so they leave it with more energy than when they enter? To overcome the asynchrony between the particle and the SP's wave, so that the particles do not reach those regions where the oscillating field would slow them down, we propose a mechanism to accelerate the SP's by tuning their phase velocity, matching it to that of the charged particles. This change in velocity is achieved by gradually changing the separation between the interfaces. Considering a separation that changes slowly over a large propagation distance, we apply a perturbative method to solve the set of field equations of the system obtaining the electric potential as a function of position along the channel axis. We design the separation profile as a function of position along the parallel coordinate in order for the SP to accelerate together with the accelerated particles.

At the end of the chapter we make a proposal for the coupling of an optical wave to the SP via a grating at the exit of the channel. The grating coupler is a complementary part of the designed cavity and we situate it at the exit opening. We obtain analytically the field scattered by the grating using Fourier analysis of the excitation of the SP at a finite shallow sinusoidal grating. Using these results one can calculate by how much is the external electric field amplified by the coupling to find the actual electric field that accelerates the charged particles. The system has to be solved self-consistently, as the cavity shape depends on the particle acceleration which depends on the SP field, which depends in turn on the position, the intensity of the incoming light, the grating coupler and also on the shape of the cavity.

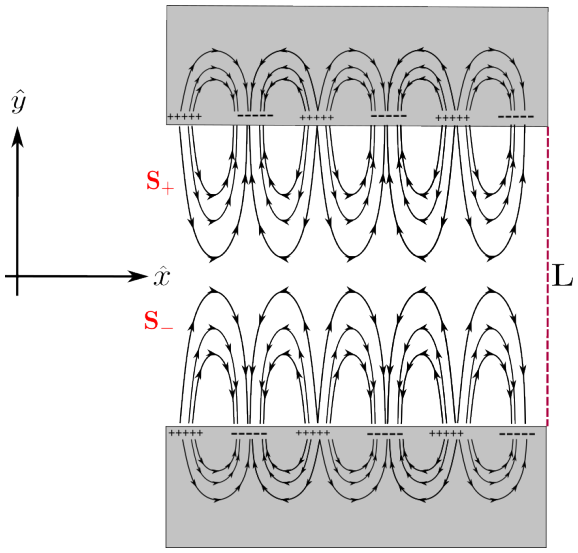

Figure 4.1: Field lines of the symmetric eigenmode of the system composed by two semi-infinite metals whose interfaces are parallel and separated by a distance L from each other. The gray part is the metal media and S_+, S_-, are the SP at the upper and lower metallic interfaces respectively.

4.1. Parallel Metallic Plates: Non-retarded Solution

Consider two semi-infinite metals bordered by flat surfaces which are parallel and separated by a distance L. Along each surface a surface plasmon $S_\pm$, such as that in Fig. 3.1, propagates, as illustrated in Fig. 4.1. When the separation L between interfaces is comparable to or smaller than the decay length of the interfaces modes, interactions between S_+, S_- give rise to coupled modes. We study the field that propagates in the space between the metals, $\boldsymbol{E}_v(x,t)$. We assume that the surface plasmon has p or *transverse magnetic* (TM) polarization, i.e., $\boldsymbol{H}$ is assumed to be in the $\hat{z}$ direction, perpendicular to the xy plane, which we take as the incidence plane, on which the electric field lies.

In the non-retarded limit the oscillation time is assumed to be long compared to the time it takes for light to cover other relevant distances, such as the plasmon wavelength $\lambda_{\rm SP}$, thus the wavelength λ in vacuum is assumed much greater than $\lambda_{\rm SP}$. This is equivalent to assuming the validity of the limit $c \to \infty$, so that the field equations become those corresponding to the electrostatic regime. Thus, the equation to solve is the Laplace equation within the homogeneous regions,

$$\nabla^2\Phi(x,t) = 0, \quad y < -L/2,\ -L/2 < y < L/2 \quad \text{or} \quad L/2 < y \tag{4.1}$$

with the following boundary conditions at the interfaces,

$$\begin{aligned} E_x(x, y = \pm L/2 + \nu, t) &= E_x(x, y = \pm L/2 - \nu, t) \\ D_y(x, y = \pm L/2 + \nu, t) &= D_y(x, y = \pm L/2 - \nu, t), \end{aligned} \tag{4.2}$$

where we take the limit $\nu \to 0^+$, i.e., a vanishingly small positive quantity, together with the asymptotic condition of convergent fields at $y \to \pm\infty$. We then use the *ansatz*

$$\Phi(x,y,t) = \phi(y)e^{i(Qx-\omega t)}. \tag{4.3}$$

Substituting it in Eq. (4.1) we obtain an ordinary linear differential equation for $\phi(y)$ with the general solution

$$\phi(y) = \phi_+ e^{Qy} + \phi_- e^{-Qy} \tag{4.4}$$

within each region.

Applying the convergence conditions at $\pm\infty$ we get expressions for the potential in the three regions

$$\phi(y) = \begin{cases} B_m e^{-Qy} & \text{if } L/2 < y, \\ A_v e^{Qy} + B_v e^{-Qy} & \text{if } -L/2 < y < L/2, \\ A_m e^{Qy} & \text{if } y < -L/2. \end{cases} \tag{4.5}$$

Using the continuity at each interface, which we rewrite in terms of the potential as $\phi(\pm L/2 \pm \nu) = \phi(\pm L/2 \mp \nu)$, $\epsilon_m \partial_y \phi(y = L/2 + \nu) = \epsilon_d \partial_y \phi(y = L/2 - \nu)$, and $\epsilon_m \partial_y \phi(y = -L/2 - \nu) = \epsilon_d \partial_y \phi(y = -L/2 + \nu)$, we can eliminate A_m and B_m and obtain a system of equations for A_v and B_v,

$$\underbrace{\begin{pmatrix} -(1+\epsilon_m) & e^{-QL}(1-\epsilon_m) \\ -e^{-QL}(1-\epsilon_m) & (1+\epsilon_m) \end{pmatrix}}_{R} \begin{pmatrix} A_v \\ B_v \end{pmatrix} = 0, \tag{4.6}$$

where we've set the dielectric function of the space between interfaces $\epsilon_d = \epsilon_v = 1$, and ϵ_m is the dielectric function of the metals. The non trivial solutions are given by $\det(R) = 0$, where R is the matrix introduced in Eq. (4.6), from which we find the dispersion relations

$$Q = \frac{1}{L}\ln(\pm\Lambda) = \frac{1}{L}\ln\left(\pm\frac{(1-\epsilon_m)}{(1+\epsilon_m)}\right). \tag{4.7}$$

The plus sign corresponds to a symmetric mode $A_v = B_v$, $A_m = B_m$ and the minus sign to an antisymmetric mode $A_v = -B_v$, $A_m = -B_m$. Notice that Q depends on the frequency through the dielectric function ϵ_m and on the separation L between the interfaces. The dispersion relations are illustrated in Fig. 4.2 assuming the Drude model for the conductors.

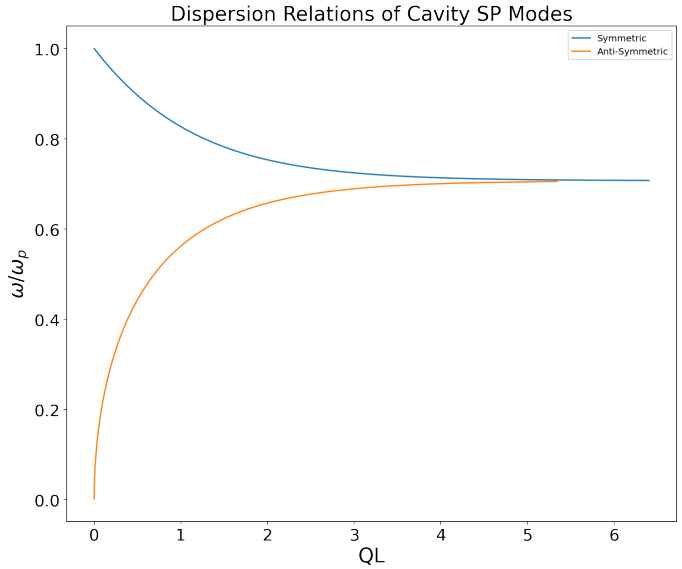

Figure 4.2: Dispersion relations of the surface plasmon modes of a metal-vacuum-metal structure in the non-retarded limit using the Drude model. The lower line is associated to the anti-symmetric and the upper one to the symmetric mode. The frequency is normalized with the plasma frequency and the wavevector with the separation distance between the metal interfaces.

Since the two potential solutions in the space between the interfaces, are such that $A_v = \pm B_v \equiv$

$\pm A/2$, the symmetric and anti-symmetric cases, can be written as

$$\phi(y) = \begin{cases} A\cosh(Qy) & \text{symmetric,} \\ A\sinh(Qy) & \text{anti-symmetric,} \end{cases} \quad \text{if } -L/2 < y < L/2. \tag{4.8}$$

4.1.1. Force Fields of the Eigenmodes

Consider the same system as in Fig. 4.1 and suppose a charged particle lies halfway between the interfaces on which an eigenmode is propagating. The particle will experiences the oscillatory force due to its interaction with the electric field of the eigenmode. Both modes symmetric and anti-symmetric are shown in Fig. 4.3.

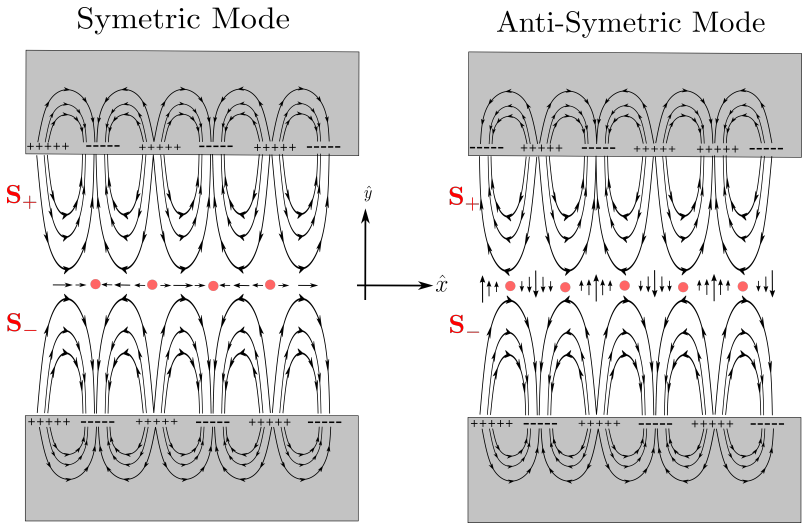

Figure 4.3: Lines of force felt by a positive charged particle immersed in the system's electromagnetic field and lying just at the middle of the channel. There are two modes but only the symmetric one can accelerate the particle along its propagation direction.

As the anti-symmetric mode has a null parallel component of the electric field at the center of the channel, it is not an option for our purposes. Nevertheless the symmetric mode has a finite parallel component, as can be seen in the figure.

4.2. Acceleration for the Symmetric Mode

Suppose that the symmetric mode is excited and that a particle with charge q and mass m is placed at some time at a position where the field has some phase θ_0. The question is, how do we keep the particle and the field synchronized as the particle is accelerated by the field and the field propagates along the channel? In this section we propose to change the mode's phase velocity by gradually changing the distance between the interfaces. For this, we solve the electrostatic equations perturbatively using the potential obtained in the previous section 4.1 but with an amplitude and phase that changes with the position as does the separation between the interfaces.

4.2.1. Channel with a Gradually Varying Width

Consider the metal-vacuum-metal system, but now with a slowly changing separation $L(x)$ dependent on x, i.e., varying along the axis of the channel. Since we obtained for parallel plates that

the wavenumber Q is a function of the separation beteween the interfaces Eq. (4.7), it will become x-dependent as well, $Q(x) = \frac{1}{L(x)} \ln\left(\frac{1-\epsilon_m}{1+\epsilon_m}\right)$. Therefore, we use this relation to gradually accelerate the SP.

We will use the potential previously obtained for a constant separation to build an *ansatz* for the solution with a varying separation,

$$\Phi(x,y,t) = \phi_s(x) e^{i\left(\int_{x_0}^{x} Q(x')dx' - \omega t\right)} \cosh\left(Q(x)y\right). \tag{4.9}$$

We expect ϕ_s to depend also on y, but as we chose the even solution, its first y-derivative at $y = 0$ would vanish.

Assuming that $\phi_s(x)$ is a slowly varying function of x, substituting Eq. (4.9) in Laplace equation, and doing a lot of algebraic manipulation, as detailed in the Appendix A, we obtain the second derivatives with respect to position of this potential,

$$\begin{aligned}\partial_x^2\Phi(x,y,t) = e^{i\int_{x_0}^{x} Q(x')dx'}(\partial_x^2\phi_s(x))(\cosh\left(Q(x)y\right)) + \partial_x\phi_s(x)\Big[2iQ(x)\cosh(Q(x)y) \\ +2y(\partial_x Q(x))\sinh(Q(x)y)\Big] + \phi_s(x)\Big\{-(Q(x))^2\cosh\left(Q(x)y\right) \\ +(\partial_x Q(x))\Big[2iQ(x)y\sinh\left(Q(x)y\right) + i\cosh\left(Q(x)y\right) + y^2(\partial_x Q(x))\cosh\left(Q(x)y\right)\Big]\Big\},\end{aligned} \tag{4.10a}$$

$$\begin{aligned}\partial_y^2\Phi(x,y,t) =& \partial_y\left(\phi_s(x)e^{i\int_{x_0}^{x} Q(x')dx'}Q(x)\sinh\left(Q(x)y\right)\right) \\ =& \left(\phi_s(x)e^{i\int_{x_0}^{x} Q(x')dx'}(Q(x))^2\cosh\left(Q(x)y\right)\right).\end{aligned} \tag{4.10b}$$

Neglecting products of spatial derivatives of slowly varying terms and second derivatives we approximate the Laplacian as

$$\begin{aligned}\nabla^2\Phi(x,y,t) = \partial_x^2\Phi(x,y,t) + \partial_y^2\Phi(x,y,t) \\ = \partial_x\phi_s(x)\Big[2iQ(x)\cosh\left(Q(x)y\right)\Big] + \phi_s(x)\partial_x Q(x)\Big[2iQ(x)y\sinh\left(Q(x)y\right) + i\cosh(Q(x)y)\Big].\end{aligned} \tag{4.11}$$

Taking the limit $y \to 0$, i.e restricting the solution to the center of the channel, we arrive at a simplified equation for the amplitude,

$$2(\partial_x\phi_s(x))Q(x) + \phi_s(x)(\partial_x Q(x)) = 0, \tag{4.12}$$

with solution

$$\phi_s(x) = \sqrt{\frac{Q_0}{Q(x)}}\phi_0, \tag{4.13}$$

i.e., the amplitude of the potential is inversely proportional to the square root of the local wave vector $Q(x)$, which in turn depends on the separation $L(x)$ between the interfaces, which is a function of x. $Q_0 = Q(x_0)$ and $\phi_0 = \phi(x_0)$ are determined from initial conditions at a given but arbitrary position x_0. Substituting Eq. (4.9) into the *ansatz*, we obtain the potential along the axis of the channel,

$$\Phi(x, y=0, t) = \phi_0\sqrt{\frac{Q_0}{Q(x)}}e^{i(\int_{x_0}^{x} Q(x')dx' - \omega t)}. \tag{4.14}$$

Now, let's consider a particle accelerated along the channel by the field of the SP. If it moves with a velocity that differs from the phase velocity of the SP, the phase of the field at the location of the particle would change in time, so it would decelerate at some times instead of accelerating. To avoid this, we want the SP to accelerate with the particle, so the velocities of the particle and the wave match each other. We also want this situation to be stable, so that particles that start with slightly different velocities or position are also synchronously accelerated.

4.2.2. Synchronous Motion: Analytical Solution

In the nonrelativistic case, the particle's equation of motion is Newton's second law. We analyze now the motion along the channel's axis, i.e., along x, at the mid-plane between the interfaces. The explicit form of the electric field is derived from $\boldsymbol{E}(x,t) = -\nabla\Phi(x,t)$. Sustituting Eq. (4.14) and keeping just the dominant terms, we obtain

$$\begin{aligned} E_x(x,t) =& \mathrm{Re}(-i\phi_0\sqrt{Q_0}\sqrt{Q(x)}e^{i(\int_{x_0}^{x} Q(x')dx' - \omega t)}), \\ =& \mathrm{Re}(E_0\sqrt{\frac{Q(x)}{Q_0}}e^{i(\int_{x_0}^{x} Q(x')dx' - \omega t)}) \end{aligned} \tag{4.15}$$

where $E_0 = -i\phi_0 Q_0$ is the amplitude of the electric field at x_0. Assuming $E_0 = |E_0|e^{i\theta_0}$, the phase of the electric field at any position and time is

$$\Theta(x,t) = \left(\int_{x_0}^{x} Q(x')dx' - \omega t\right) + \theta_0. \tag{4.16}$$

Given the field by Eq. (4.15), the acceleration $\ddot{x}$ of a particle of charge q at a position $x(t)$ is

$$\ddot{x}(t) = \frac{q}{m}E_x(x(t),t). \tag{4.17}$$

We first solve the dynamics of a particle for which the field keeps a constant phase $\Theta(x(t),t) = \theta_i$ as it evolves, namely a nominal particle injected at position x_i at time $t = 0$. Since x_0 is an arbitrary position, we chose it to be equal to the injection point of the nominal particle $x_i = x_0$, hence, $E_0 = E_i = -i\phi_i Q_i$ and $\theta_0 = \theta_i$. Thus, for this particle, Eq. (4.17) is

$$\ddot{x}(t) = \frac{q}{m}|E_i|\sqrt{\frac{Q(x(t))}{Q_i}}\cos\theta_i. \tag{4.18}$$

To keep $\Theta(x(t),t) = \theta_i$ constant, the particle and the plasmon should move in synchrony, i.e., the phase velocity of the SP should be equal to the particle's velocity,

$$\dot{x}(t) = v(\text{particle}) = v(\text{plasmon}) = \frac{\omega_{\mathrm{SP}}}{Q(x(t))} = v_p(t). \tag{4.19}$$

Deriving,

$$\dot{v}_p(t) = -\frac{\omega_{\mathrm{SP}}}{Q^2(x)}\left(\frac{dQ(x)}{dx}\right)\underbrace{\left(\frac{dx(t)}{dt}\right)}_{v_p = \frac{\omega_{\mathrm{SP}}}{Q(x)}} = -\frac{\omega_{\mathrm{SP}}^2}{Q^3(x(t))}\left(\frac{dQ}{dx}\right). \tag{4.20}$$

Using Eq. (4.7),

$$\left(\frac{dQ(x)}{dx}\right) = -\ln(\Lambda)\frac{1}{L^2(x)}\left(\frac{dL}{dx}\right), \tag{4.21}$$

where Q is written as $Q(x) = \ln(\Lambda)/L(x)$, and $\Lambda = (1-\epsilon_m)/(1+\epsilon_m)$ as in Eq. (4.7). The SP acceleration may be written in terms of $L(x)$ as

$$\dot{v}_p(t) = \left(\frac{\omega_{\mathrm{SP}}}{\ln\Lambda}\right)^2\left(\frac{dL}{dx}\right)L(x). \tag{4.22}$$

Equating the SP acceleration Eq. (4.22) to the particle acceleration Eq. (4.18), we obtain

$$\ddot{x}(t) = \frac{q}{m}|E_i|\sqrt{\frac{Q(x)}{Q_i}}\cos\theta_i = \left(\frac{\omega_{\mathrm{SP}}}{\ln\Lambda}\right)^2\left(\frac{dL(x)}{dx}\right)L(x) = \frac{q}{m}|E_i|\sqrt{\frac{\ln\Lambda}{Q_i L(x)}}\cos\theta_i. \tag{4.23}$$

This is a differential equation for $L(x)$ which may be integrated,

$$\int_{L_i}^{L} dL(L)^{3/2} = \frac{q}{m}|E_i|\sqrt{\frac{\ln\Lambda}{Q_i}}\cos\theta_i\left(\frac{\ln\Lambda}{\omega_{\rm SP}}\right)^2\int_0^x dx'. \tag{4.24}$$

We set $x_i = 0$. The corresponding separation $L_i = L(x_i) = L(0)$ is determined by the initial velocity of the nominal particle. Integrating both sides we obtain

$$\frac{2}{5}(L^{5/2}(x) - L_i^{5/2}) = \frac{q}{m}|E_i|\cos\theta_i\sqrt{\frac{\ln\Lambda}{Q_i}}\left(\frac{\ln\Lambda}{\omega_{\rm SP}}\right)^2 x, \tag{4.25}$$

from which we find the profile

$$L(x) = \left(\frac{5}{2}\frac{q}{m}|E_i|\sqrt{\frac{\ln\Lambda}{Q_i}}\cos\theta_i\left(\frac{\ln\Lambda}{\omega_{\rm SP}}\right)^2 x + L_i^{5/2}\right)^{2/5}. \tag{4.26}$$

Notice that in our nonretarded calculation $Q(x)$ is inversely proportional to $L(x)$, i.e., $Q(x)L(x) = \ln\Lambda$ is a constant. This allows us to rewrite the solution as

$$\begin{aligned} L(x) &= \left(\frac{5}{2}\frac{1}{\xi^2}\cos\theta_i\,\eta Q_i L_i^{5/2}x + (L_i)^{5/2}\right)^{2/5}, \\ L(x) &= \left(\frac{5}{2}\frac{1}{\xi^2}\cos\theta_i\,\eta Q_i x + 1\right)^{2/5} L_i, \end{aligned} \tag{4.27}$$

where we substituted $\ln\Lambda = Q_i L_i$ and introduced the dimensionless quantities

$$\xi = \omega_{\rm SP}/\omega_p \tag{4.28}$$

and

$$\eta = \frac{q}{m}|E_i|\left(\frac{Q_i}{\omega_p^2}\right). \tag{4.29}$$

The separation $L(x)$ obtained above corresponds to a particle perfectly synchronized with the system's mode, given its chosen initial conditions and a suitable θ_i. The channel profile $L(x)$, is shown in Fig. 4.4, where the point where the particles are injected is indicated, as well as the variable separation between interfaces. Portions of the boundary are yet undefined, as they depend on the mechanisms of injection and excitation, but the extrapolated profile is indicated by dashed lines. The vertex of the cavity at x_v is defined by $L(x_v) = 0$ and corresponds to the dashed region, where, furthermore, our approximation of a gradual varying cavity doesn't hold.

4.2.3. Non-Nominal Motion: Stability

Using Eq. (4.26) we may study the dynamics of particles which are not in perfect sync with the plasmon field, that is, particles with initial conditions which do not match those of the nominal particle. First we need to obtain the phase of the field at any position and time, $\Theta(x(t), t)$, which we obtain from from Eq. (4.16) substituting x_0 and θ_0 by x_i and θ_i. To that end, we need the explicit dependence of $Q(x)$ in x,

$$Q(x) = \frac{\ln\Lambda}{L(x)} = \frac{Q_i}{1 + \left(\frac{5}{2}\frac{1}{\xi^2}\cos\theta_i\,\eta Q_i x\right)^{2/5}}. \tag{4.30}$$

We perform the integral in Eq. (4.16) by changing integration variable to $s = 1 + (5\cos\theta_i\,\eta Q_i x)/2\xi^2$, $ds = 5\cos\theta_i\,\eta Q_i dx/2\xi^2$, yielding

$$\Theta(x,t) = \frac{2}{3}\frac{\xi^2}{\cos\theta_i\,\eta}\left[\left(\frac{L(x)}{L_1}\right)^{3/2} - 1\right] + \theta_i - \omega t. \tag{4.31}$$

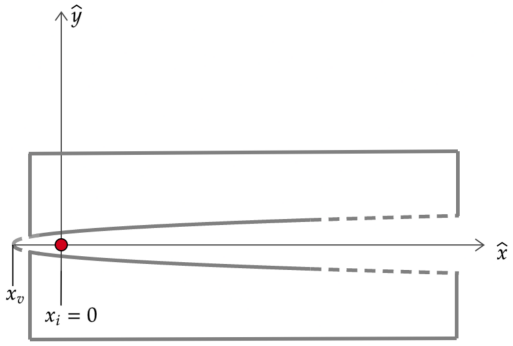

Figure 4.4: Cavity design obtained from the syncrhonous motion condition of a nominal particle with the surface plasmon. x_v is the vertex coordinate given by $L(x_v) = 0$, $x_i = 0$ is the injection point of charged particles and $L(x)$ the variable distance between interfaces. The dashed lines are extrapolations onto undefined parts of the boundary of the cavity which are to be designed by the mechanism chosen for the injection of particles and the excitation of the SP. The vertical and horizontal scales depend on design parameters.

The field at any position x and time t within the cavity is

$$E_x(x,t) = |E_i|\sqrt{\frac{Q(x)}{Q_i}}\cos\Theta(x,t). \tag{4.32}$$

The acceleration of any particle is

$$\begin{aligned}\ddot{x}(t) &= \frac{q}{m}|E_i|\sqrt{\frac{Q(x(t))}{Q_i}}\cos\Theta(x(t),t) \\ &= \eta\sqrt{\frac{Q(x(t))}{Q_i}}\cos\Theta(x(t),t)\frac{\omega_p^2}{Q_i}.\end{aligned} \tag{4.33}$$

A numerical integration of Eq. (4.33) using, for example, the Runge-Kutta-Nystrom method, may be performed to obtain the trajectories in configuration and phase space for particles with arbitrary initial conditions $x(t_i)$ and $\dot{x}(t_i)$ at arbitrary injection times t_i using the analytical formulas we've shown above. The results can show us how stable is our system against perturbations in the initial conditions that differ along the nominal propagation direction from those of the nominal particle for which the channel is designed.

4.3. Excitation of the Cavity Surface Plasmon Mode

In this section we study how to excite the surface plasmons of our cavity. To that end, let's consider a metal-insulator-metal structure made up of two semiinfinite metals separated by vacuum with flat parallel interfaces a nominal distance L apart. In order to couple the symmetric SP to incoming light, we replace opposing strips of width $2a$ of these interfaces by symmetrical gratings with sinusoidal profiles of amplitude h and wavelength λ_N, as shown in Fig. 4.5. The height of the interfaces is given by

$$y_\pm(x) = \pm(L/2 + \zeta(x)) = \pm(L/2 + h\cos(Gx)\Theta(a - |x|)), \tag{4.34}$$

where $G = 2\pi/\lambda_N$ is a reciprocal vector and $2a$ is the length of the grating. Here, $\Theta(\ldots)$ is the unit Heavyside step function. For convenience, we changed our origin $x = 0$ to the center of the gratings.

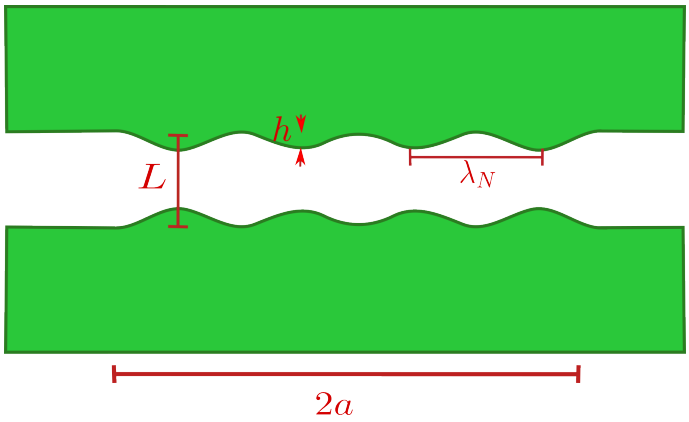

Figure 4.5: Sinusoidal gratings to excite the SP using light. Two semiinfinite metals delimited by flat surfaces except for a strip with a sinusoidal profile with amplitude h and period $\lambda_N = 2\pi/G$. The interfaces are parallel and separated by a nominal distance L. The rough strips have a width $2a$.

Since the rough region has a finite extent along x, (Eq. (4.34)), it is not periodic, so we take its Fourier transform

$$\zeta(x) = \int_{-\infty}^{\infty} \frac{dQ}{2\pi} \zeta_Q e^{iQx} \tag{4.35}$$

to write it as a superposition of periodic contributions. The Fourier coefficients ζ_Q are given by

$$\begin{aligned} \zeta_Q =& h \int_{-a}^{a} dx \cos(Gx) e^{-iQx} = \frac{h}{2} \int_{-a}^{a} dx (e^{i(G-Q)x} + e^{-i(G+Q)x}) \\ =& ha \left(\mathrm{sinc}((G-Q)a) + \mathrm{sinc}((G+Q)a)\right). \end{aligned} \tag{4.36}$$

We assume the period λ_N is much smaller than the free-space wavelength of light λ, so that we may use a nonretarded approximation. Thus, we excite the system with p polarized light propagating vertically with a field $\boldsymbol{E}_{\mathrm{ext}}$ along the horizontal direction x, which we take as approximately position-independent. We solve the cuasi-static induced potential looking for the symmetric solution with non-zero electric field along the channel. We propose an induced potential ϕ given in each homogeneous region as a superposition of solutions of Laplace's equation, in analogy to Rayleigh's treatment of diffraction by a grating [43],

$$\phi_{\mathrm{ind}}(x,y) = \begin{cases} \int_{-\infty}^{\infty} \frac{dQ}{2\pi} \alpha_{vQ} e^{iQx} \cosh(|Q|y) & -\frac{L}{2} - \zeta(x) < y < \frac{L}{2} + \zeta(x), \\ \int_{-\infty}^{\infty} \frac{dQ}{2\pi} \alpha_{mQ} e^{iQx} e^{-|Q||y|} & \pm y > \frac{L}{2} + \zeta(x), \end{cases} \tag{4.37}$$

with Fourier coefficients α_{vQ} in vacuum and α_{mQ} in both metallic regions. Taking the gradient, we obtain the electric field,

$$\boldsymbol{E}(x,y) = \boldsymbol{E}_{\mathrm{ext}} - \int_{-\infty}^{\infty} \frac{dQ}{2\pi} \alpha_{vQ} Q e^{iQx} \begin{pmatrix} i\cosh(Qy) \\ \sinh(Qy) \\ 0 \end{pmatrix}, \qquad -\frac{L}{2} - \zeta(x) < y < \frac{L}{2} + \zeta(x), \tag{4.38}$$

$$\boldsymbol{E}(x,y) = \boldsymbol{E}_{\mathrm{ext}} - \int_{-\infty}^{\infty} \frac{dQ}{2\pi} \alpha_{mQ} Q e^{iQx} e^{-|Q||y|} \begin{pmatrix} i \\ \mp 1 \\ 0 \end{pmatrix}, \qquad \pm y > \frac{L}{2} + \zeta(x). \tag{4.39}$$

The following calculations are performed up to linear order in the small height h. The normal to the interfaces is obtained from the gradient of Eq. (4.34),

$$\hat{n}_{\pm}(x) = (-\partial_x \zeta(x), \pm 1) = (Gh \sin(Gx)(\Theta(a - |x|), \pm 1), \tag{4.40}$$

where the upper (lower) sign corresponds to the upper (lower) interface. In terms of its Fourier transform, it becomes

$$\hat{n}_{\pm} = \left(- \int_{-\infty}^{\infty} \frac{dQ}{2\pi} iQ\zeta_Q e^{iQx}, \pm 1 \right) \tag{4.41}$$

where ζ_Q is given by Eq. (4.36). The continuity of the projection of the electric field parallel to the interfaces yields simply

$$\alpha_{mQ} = \alpha_{vQ} \cosh\left(|Q| \frac{L}{2} \right) e^{|Q|\frac{L}{2}}. \tag{4.42}$$

The continuity of the perpendicular component of the displacement may be expressed as

$$\begin{gathered} \epsilon_m \hat{n}(x) \cdot \nabla\phi(x, \frac{L}{2} + \zeta(x) + \eta) = \hat{n} \cdot \nabla\phi(x, \frac{L}{2} + \zeta(x) - \eta), \\ \epsilon_m \left(-\zeta_Q iQ, 1 \right) \cdot \left(-E_{\text{ext}} + iQ\alpha_{mQ} e^{-|Q|y}, -|Q|\alpha_{mQ} e^{-|Q|y} \right) \Big|_{y_+} = \\ \left(-\zeta_Q iQ, 1 \right) \cdot \left(-E_{\text{ext}} + iQ\alpha_{vQ} \cosh\left(|Q|y \right), |Q|\alpha_{vQ} \sinh\left(|Q|y \right) \right) \big|_{y_+}, \end{gathered} \tag{4.43}$$

which yields

$$\alpha_{mQ} = -\frac{iE_{\text{ext}}(1-\epsilon_m) e^{|Q|\frac{L}{2}} \zeta_Q}{\tanh(|Q|L/2) + \epsilon_m}, \tag{4.44a}$$

$$\alpha_{vQ} = -\frac{iE_{\text{ext}}(1-\epsilon_m) \operatorname{sech}(QL/2) \zeta_Q}{\tanh(|Q|L/2) + \epsilon_m}. \tag{4.44b}$$

Notice that these amplitudes have a pole at $Q = \pm Q_{\text{SP}}$, where

$$\epsilon_m + \tanh(Q_{\text{SP}} L/2) = 0, \tag{4.45}$$

corresponds to the resonant coupling to the surface plasmon, i.e., is equivalent to Eq. (4.7). Thus, we consider only wavevectors close to the resonance, for which

$$(\epsilon_m + \tanh(QL/2)) \approx \frac{L}{2} \operatorname{sech}^2(Q_{\text{SP}} L/2)(Q \mp Q_{\text{SP}}), \quad Q \approx \pm Q_{\text{SP}}. \tag{4.46}$$

Due to the dissipation within the metal, the corresponding pole Q_{SP} corresponding to a real frequency is a complex quantity. We choose the reciprocal vector G of the grating as the real part of Q_{SP} to attain the largest coupling of the incoming field to the SP. Since the amplitudes in Eqs. (4.44) are large only around their poles, we evaluate the relatively slowly varying terms at $\pm G$ very close to resonance and replace the denominators by the expansion Eq. (4.46), giving

$$\alpha_{mQ} = \frac{-2iE_{\text{ext}} \zeta_G (1-\epsilon_m) e^{|G|L/2}}{L \operatorname{sech}^2(Q_{\text{SP}} L/2)} \left[\frac{1}{(Q - Q_{\text{SP}})} + \frac{1}{(Q + Q_{\text{SP}})} \right], \tag{4.47a}$$

$$\alpha_{vQ} = \frac{-2iE_{\text{ext}} \zeta_G (1-\epsilon_m) \operatorname{sech}(GL/2)}{L \operatorname{sech}^2(Q_{\text{SP}} L/2)} \left[\frac{1}{(Q - Q_{\text{SP}})} + \frac{1}{(Q + Q_{\text{SP}})} \right]. \tag{4.47b}$$

Substituting these amplitudes in Eqs. (4.38) and integrating in the complex plane around the singularities at $\pm Q_{\text{SP}}$ using the Cauchy integral theorem, we find the electric field within the

cavity,

$$\boldsymbol{E}(x,y) = \boldsymbol{E}_{\text{ext}} - \frac{-2iE_{\text{ext}}\zeta_G\,(1-\epsilon_m)\,\text{sech}\,(GL/2)}{L\,\text{sech}^2(Q_{\text{SP}}L/2)}\times$$
$$\begin{pmatrix} iG\cosh(Gy)\underbrace{\displaystyle\int_{-\infty}^{\infty}\frac{dQ}{2\pi}\left(\frac{e^{iGx}}{Q-Q_{\text{SP}}}-\frac{e^{-iGx}}{Q+Q_{\text{SP}}}\right)}_{(2i\sin(Gx)i\pi)/2\pi} \\ G\sinh(Gy)\underbrace{\displaystyle\int_{-\infty}^{\infty}\frac{dQ}{2\pi}\left(\frac{e^{iGx}}{Q-Q_{\text{SP}}}+\frac{e^{-iGx}}{Q+Q_{\text{SP}}}\right)}_{(2\cos(Gx)i\pi)/2\pi} \\ 0 \end{pmatrix}, \quad \text{vacuum.} \tag{4.48}$$

In order to consider the nonresonant terms as slowly varying quantities compared to the width of the SP resonance, the width of the sinc functions in Eq. (4.36), $2\pi/a$, must be much larger than the width of the resonance $\Delta Q = 2Q''_{\text{SP}} = 2/L_{\text{SP}}$. Thus, the propagation length of the plasmon should be much larger than the length of the grating $a \ll L_{\text{SP}}$.

Substituting the Fourier coefficients (Eq. (4.36)) $\zeta_{\pm G} = ha(1+\text{sinc}(2Ga))$ we rewrite the electric field as

$$\boldsymbol{E}(x,y) = \boldsymbol{E}_{\text{ext}} + e_v \begin{pmatrix} \cosh(Gy)\sin(Gx) \\ -\sinh(Gy)\cos(Gx) \\ 0 \end{pmatrix}, \quad \text{vacuum}, \tag{4.49}$$

with

$$e_v = \frac{2E_{\text{ext}}hGa(1+\text{sinc}(2Ga))(1-\epsilon_m)\,\text{sech}(GL/2)}{L\,\text{sech}^2(Q_{\text{SP}}L/2)}. \tag{4.50}$$

Similarly, from Eq. (4.39) we obtain the electric field within the metal,

$$\boldsymbol{E}(x,y) = \boldsymbol{E}_{\text{ext}} + e_m \begin{pmatrix} e^{-|G|y}\sin(Gx) \\ \mp e^{-|G||y|}\cos(Gx) \\ 0 \end{pmatrix}, \quad \pm y > \frac{L}{2} + \zeta(x), \tag{4.51}$$

where

$$e_m = \frac{2E_0h|G|a(1+\text{sinc}(2Ga))(1-\epsilon_m)e^{|G|L/2}}{L\,\text{sech}^2(Q_{\text{SP}}L/2)}. \tag{4.52}$$

The electric field depends on the amplification given by the coupling in Eq. (4.50) which depends on the height h, the reciprocal vector G, the length of the corrugated region $2a$, the separation L between interfaces, and the dielectric function of the metals ϵ_m. Since the electric field decays exponentially away from the interfaces, to have an appreciable field at the center of the channel we choose a separation L smaller than the penetration depth of the SP $L < 2/G$. Once the product GL is fixed, the dispersion relation Eqs. (4.7) and (4.45) fixes the resonant frequency and introducing dissipation, we obtain the imaginary part of the wave vector Q_{SP}. Alternatively, we rewrite Eq. (4.45) explicitly in terms of frequency using the Drude model and the complex wavevector

$$\tanh\left((Q'_{\text{SP}} + iQ''_{\text{SP}})L/2\right) + (1 - (\omega_p^2/(\omega(\omega + i/\tau)) = 0, \tag{4.53}$$

and solve it for the frequency and the imaginary part of the wavevector in terms of its real part using a root finding method. Having those parameters we can calculate the length of propagation of the SP, the dielectric function using Drude model and then the electric field along the channel.

Chapter 5

RESULTS AND DISCUSSION

Results are presented and discussed in this chapter in an order that corresponds to the analytical results of the previous chapter 4. Using the analytical results, we numerically integrate the equation of motion for different particles and compare them with those of the nominal particle to characterize the longitudinal stability of the system. We compute the SP electric field taking the limits stated before on the given values of the system's parameters. Then, analyzing and setting upper bounds to the energy gains of the injected particles in the channels we derive the device's geometry.

5.1. Longitudinal Stability

Stability of the motion along the cavity axis is analyzed by comparing the trajectories of different particles to that of the nominal particle. The nominal particle is the one that moves in synchrony with the SP so that the phase of the field at the particle's position doesn't change as it is accelerated. This constant phase, called θ_i in the last chapter, is chosen to be optimal to push particles, as shown in Fig. 5.1. We chose $\theta_i = \pi/4$ ($5\pi/4$) for positive (negative) particles. This way, particles that fall behind the nominal particle would feel a stronger force and would catch up. Similarly, particles that outrun the nominal particle would feel a weaker force, allowing the nominal particle to catch up. Thus, if a particle is delayed or jumps ahead, the phase has a broad range of values that can take, and the particles will still be accelerated.

We integrate numerically the equation of motion Eq. (4.33) using the Runge-Kutta-Nymstrong fourth order method. We normalize Eq. (4.33) to the dimensionless coefficient η so that changing

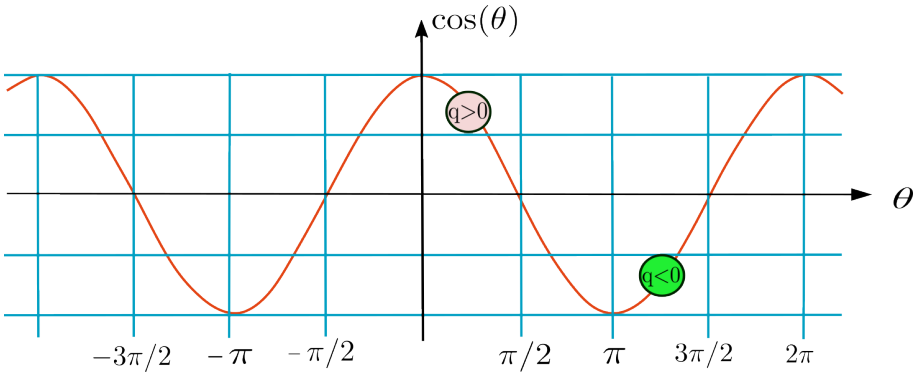

Figure 5.1: Electric field with a cosine profile along the channel showing our choice of the optimal initial phase for the nominal particle. We choose the initial phase for positive and negative charges as $\pi/4$ and $5\pi/4$ as discussed in the text.

the exciting field changes a scale factor but not the behavior of our results.

Below we show results for two cases: particles injected at a position x_i equal to that of the nominal particle but with different initial velocities than that of the SP at x_i and the paths of particles injected at different initial positions but with initial velocities equal to that of the SP at x_i. To the position x_i along the channel corresponds a separation $L(x_i) = L_i$, SP wavevector $Q_i = \ln(\Lambda)/L_i$ and SP velocity $Q_{\rm SP}/\omega$. We chose $\omega = 0.78\omega_p$ which is within the values allowed for the symmetric mode frequencies and corresponds to a wavevector $Q_{\rm SP} \approx 1.5/L$, so the field at mid-channel is quite appreciable. The results are shown in Fig. 5.2, where it can be seen that particles with initial velocities as large as four times that of the nominal particle are steadily accelerated, oscillating around the nominal trajectory, while particles with larger initial velocity are eventually left behind. Fig. 5.3 shows the corresponding results in phase space, velocity vs. position.

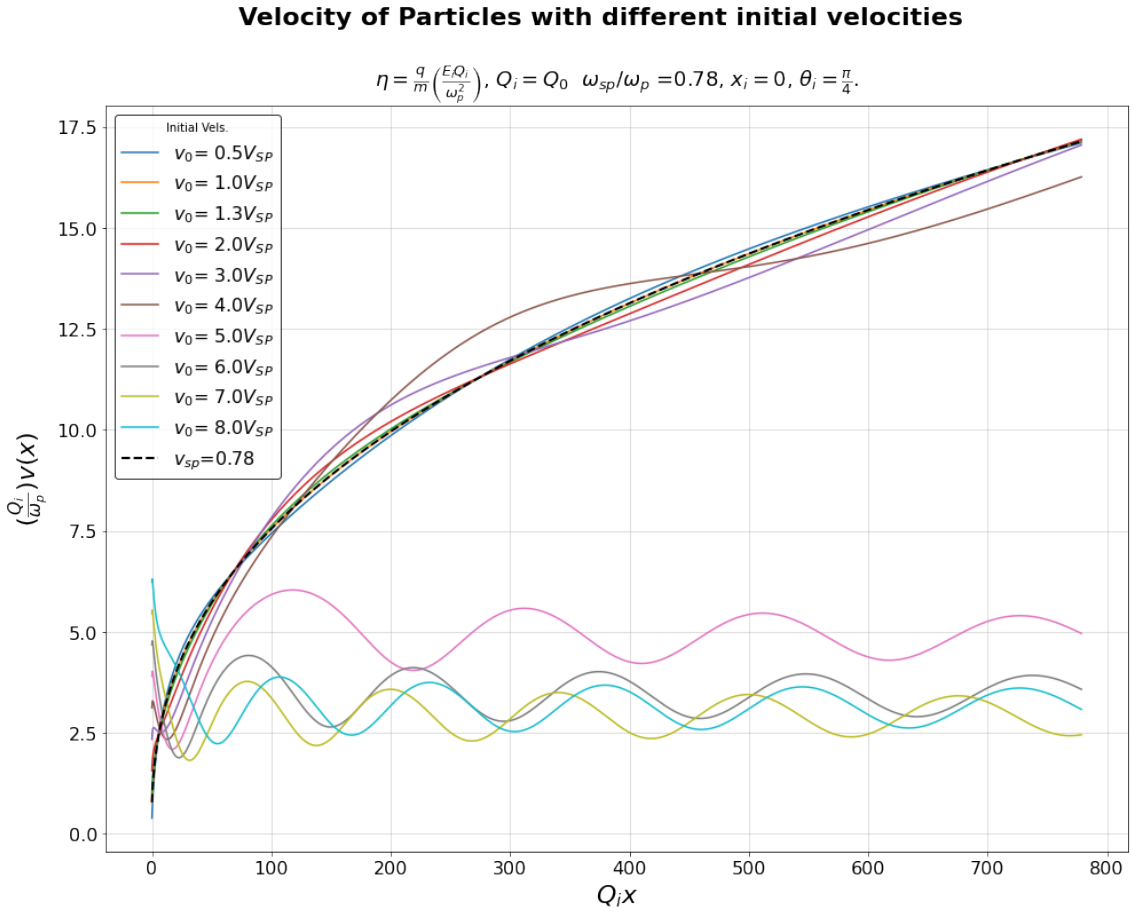

Figure 5.3: Phase space: velocity of the same particles as in Fig. 5.2 as a function of their position. The dotted black line corresponds to the nominal particle. The colored lines correspond to particles injected with different initial velocities with respect to that of the SP at the initial position x_i.

The system is stable against fluctuations in the initial velocity, as particles that get ahead feel a smaller field than the nominal particle, so they slow down relatively and are overtaken by the nominal particle, so they get into a region with a larger field and they get ahead again, repeating the cycle of decreasing and increasing acceleration around the nominal value. Persistently accelerated particles are trapped in a region where the phase differs by a small amount from the nominal phase.

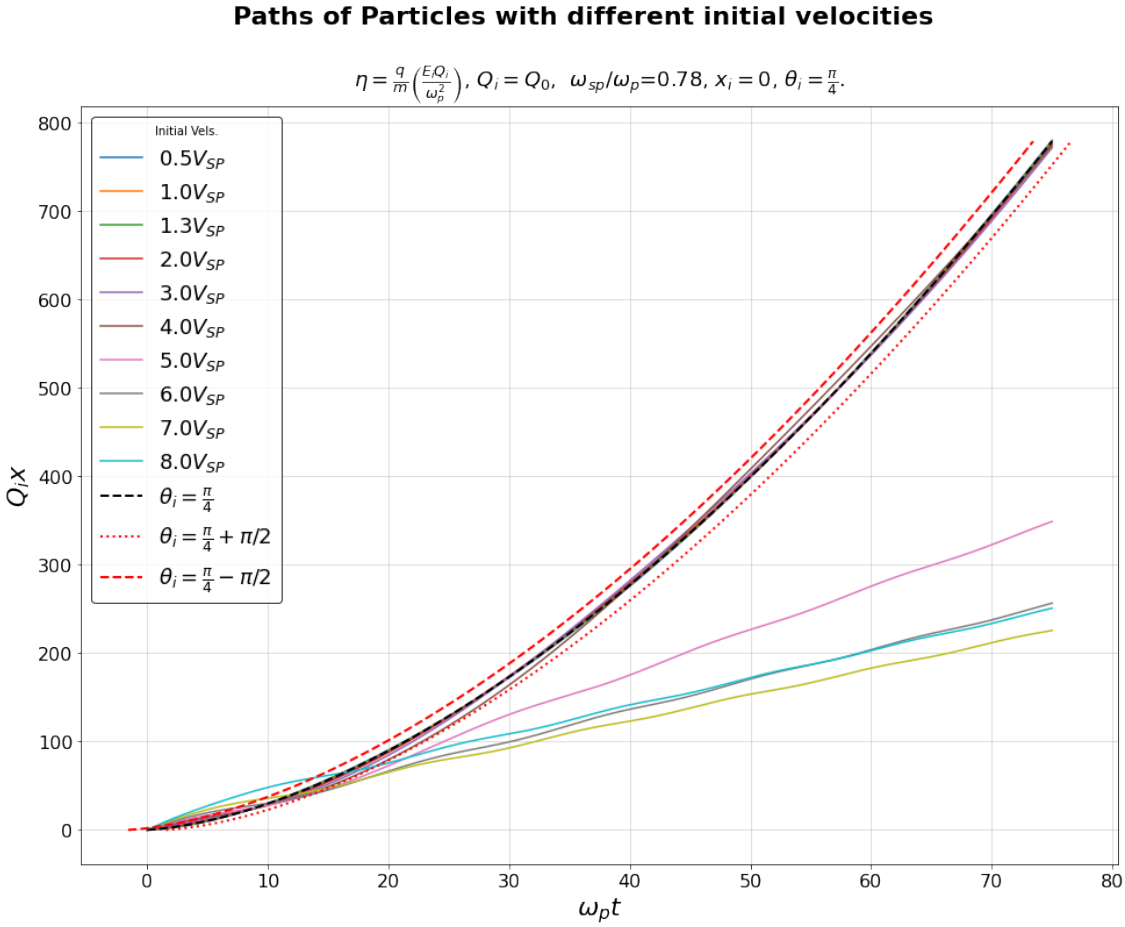

Figure 5.2: Position of various accelerated positive particles as a function of time. The position is normalized with the SP wavevector Q_i at the injection position and time is normalized with the plasma frequency ω_p. The dashed black line represents the nominal particle injected at $t = 0$ at $x_i = 0$ with a velocity ω_{SP}/Q_i and the initial phase is taken as $\theta_i = \pi/4$. The dashed and dotted red lines correspond to $\theta(x(t), t) = \pi/4 \pm \pi/2$, delayed and advanced with respect to the nominal position. The colored lines correspond to particles injected with different initial velocities $v_i(0)$ at the same initial position x_i.

Particles with initial velocities much greater than that of the SP are slowed down when they reach a region where the field has the opposite sign. Then, they slow down so much that the crest of the SP overtakes them, as when a wave overtakes a surfer, so they end up oscillating around a fixed or a slowly moving position, alternatively gaining and then losing energy from and to the oscillating field, in contrast with other particles whose energy increases continually as they travel along with the SP.

The following results show the stability against fluctuations in the initial positions. Fig. 5.4 shows position vs. time and Fig. 5.5 velocity vs. position for particles with different initial positions but the same initial velocity. It can be seen that those particles situated up to three times the inverse of the wavevector (i.e. $x \leq 3/Q_i \approx \lambda_i/2$) away from the nominal position are still accelerated by the SP, while those that are injected farther away are left behind and are not effectively accelerated.

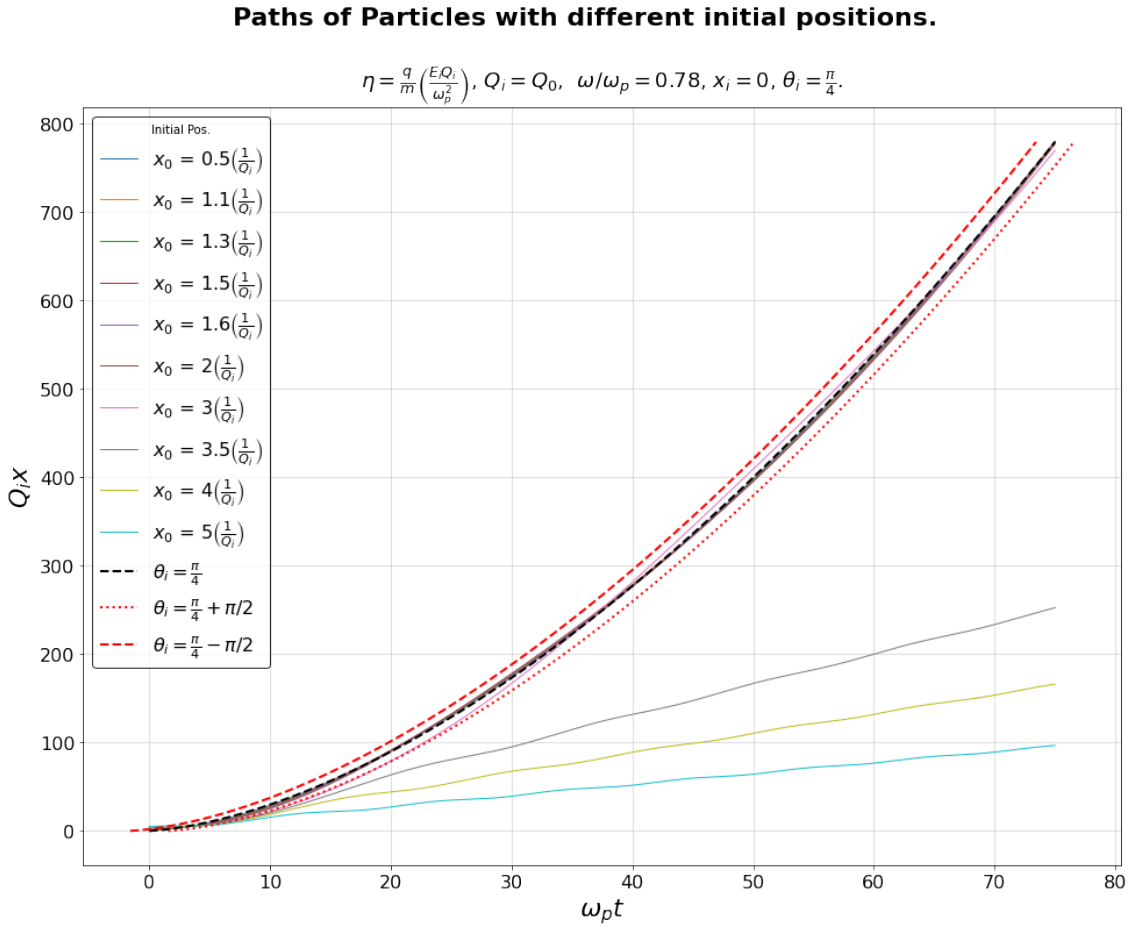

Figure 5.4: Positions of various accelerated particles as function of time, as in Fig. 5.2 but for particles with different initial positions $x(0)$ and the same initial velocity as the SP.

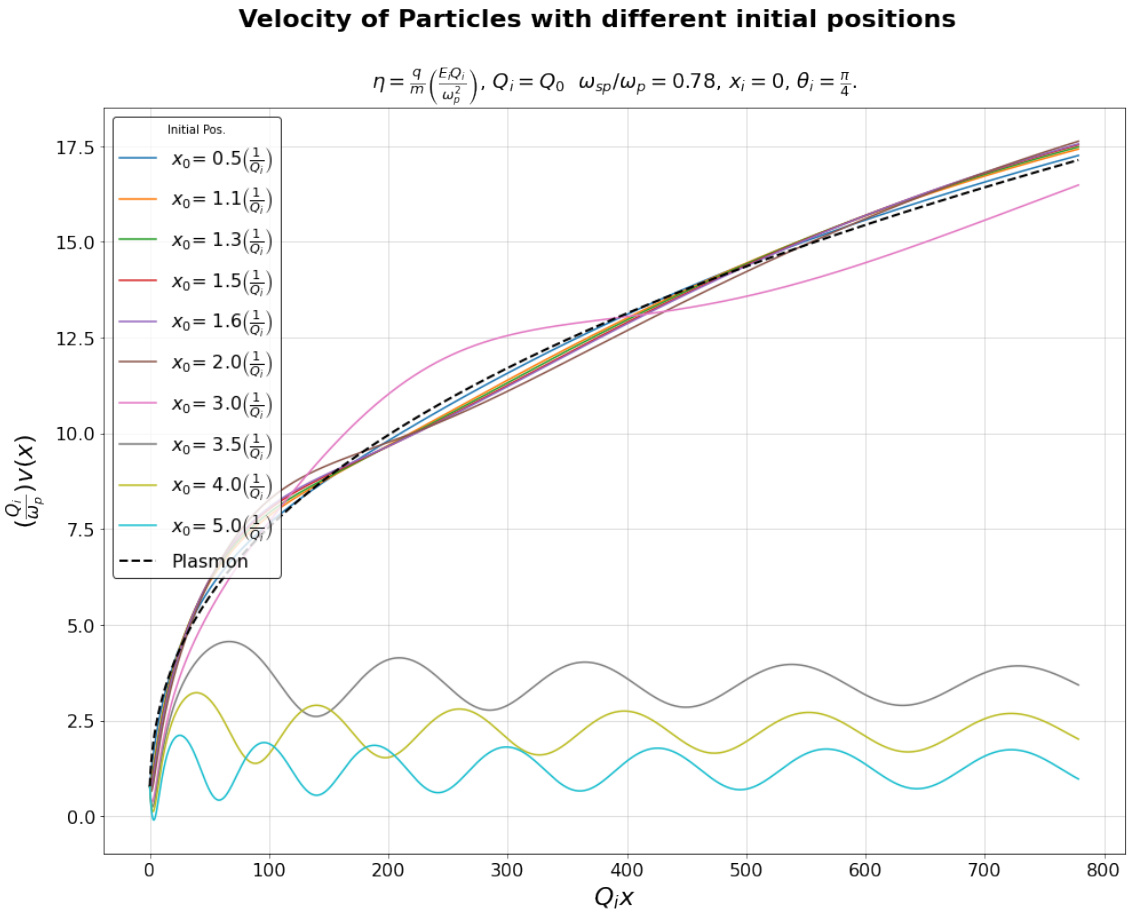

Figure 5.5: Phase space: velocities as a function of position, as in Fig. 5.3, but for particles with different initial position and the same initial velocity as the SP.

From these results we conclude that the shape $L(x)$ given by Eq. (4.26) and our choice of initial phase $\theta_i = \pi/4$ ($5\pi/4$) for positive (negative) particles yields a feasible geometry for accelerating particles using surface plasmons, and that the system has a very good stability under perturbations on the initial position and velocity of the injected particles.

5.2. Excitation of the Surface Plasmon

In Sec. 4.3 we studied the excitation of the SP using a grating coupler and we obtained expressions for the induced SP field in a channel in terms of the incident electric field (Eqs. (4.49)-(4.52)). The grating coupler and the cavity attachment would look qualitatively as in Fig. 5.6. The phase velocity of the symmetric SP is opposite to its group velocity as shown in its dispersion relation in [Fig. 4.2], the energy moves towards the left, from the exit towards the injection point of the accelerator, while its phase moves toward the right, along the acceleration direction. Thus, we chose the generation of the SP by coupling them to light at the exit of the channel, where the particles are shoot out. The grating coupler is defined by its period λ_N, corresponding to a grating wavevector $G = \frac{2\pi}{\lambda_N}$ which is chosen to be the real part of the plasmon wavevector $Q(x)$ evaluated at the exit of the cavity x_c. QL is constant and determined by the dispersion relation of the symmetric mode $QL = \ln((1-\epsilon_m)/(1+\epsilon_m))$. The frequency of the SP is chosen so that the electric field at the mid-plane between the interfaces has not decayed too much. Since we are in the non-retarded

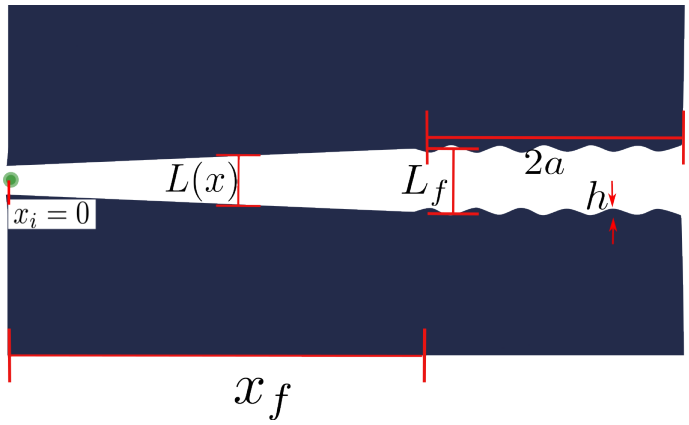

Figure 5.6: Schematic design of the channel for the co-acceleration of its SP mode and injected charged particles, and grating coupler (not to scale). The system is a MIM structure with a geometry given by Eq. (4.26) and with a sinusoidal grating imprinted near the exit from which the accelerated particles would emerge.

regime, the penetration constant is $k_v = Q'$, the penetration length is given by $\delta_v = 1/Q'$. Then the separation length shouldn't be greater than approximately $L \leq 2\delta_v \rightarrow Q'L \leq 2$. Setting for definitiveness $Q'L = QL = 1.5$, using the collision average time $\tau = 20$ fs for Ag, and the Drude model, the values of the roots of Eq. (4.53) are $\omega = 0.78\omega_p$ and the imaginary part of the wavevector $Q'' = -.022Q'$. The negative value of the imaginary part of the wavevector is consistent with a negative group velocity: the energy of the SP propagates and is dissipated towards the left while the phase travels towards the right. As we set $QL = 1.5$, then $GL_f = 1.5$, where L_f is the separation between grating interfaces at the exit of the cavity. Thus, $L_f = \frac{1.5}{2\pi}\lambda_N$. The number of periods that fit the coupler is determined by its length, $2a$. For the following results we chose a grating coupler four wavelengths long $2a = 4\lambda_N$ in order to fulfill the approximation used to arrive to Eqs. (4.47a) and (4.47b), which is that the width of the sinc functions i.e., $2\pi/a$ is much larger than the width of the resonance of the field amplitude $\Delta Q = 2Q''_{SP} = 2/L_{SP}$, so that we may approximate the sinc by a constant at resonance. Choosing a grating length much shorter than the SP propagation distance $2a \ll \pi L_{\mathrm{SP}}$ and using the imaginary part of SP wavevector, we get that $2a \ll \pi/(0.022Q') \approx 25\lambda_N$. This approximation allowed us to perform the complex integration in Eqs. (4.48). With those values, we obtained the coupling between an external field along the $\hat{x}$ axis and the SP. The total electric field inside the channel is the sum of the external electric field plus the induced field, as given in Eqs. (4.49). Fig. 5.7 shows the components of the fields induced close to the gratings, calculated through Eqs. (4.49)-(4.52) for the parameters $2a = 4\lambda_N$, $G = 2\pi/\lambda_N$, $Q'(x)L(x) = GL_f = 1.5$. Since (h/λ_N) is assumed to be a small perturbative parameter for a low-angle, low-height grating, it must be of at most order $Gh = (2\pi/\lambda_N)h \approx 0.1$. Thus, we take $h = 0.015\lambda_N$. The field then turns out to be approximately $e_v \approx 250(h/\lambda_N)E_{\mathrm{ext}} \approx 3.75E_{\mathrm{ext}}$.

The dispersion relation gives us the resonance frequency and the imaginary part of the SP's wavevector, so we can know how long does the SP propagate along the cavity. The solution using an average time between collisions of Ag $\tau \approx 20$ fs in the Drude model gives us $Q''\lambda_N = -0.14$. The propagation distance of the SP is then $L_{\mathrm{SP}} = 1/|Q''| \approx 7.1\lambda_N$. This propagation distance turns out to be less than an order of magnitude larger than the SP's wavelength, for the parameters chosen above. This shortcomming is discussed below in Sec. 5.3.

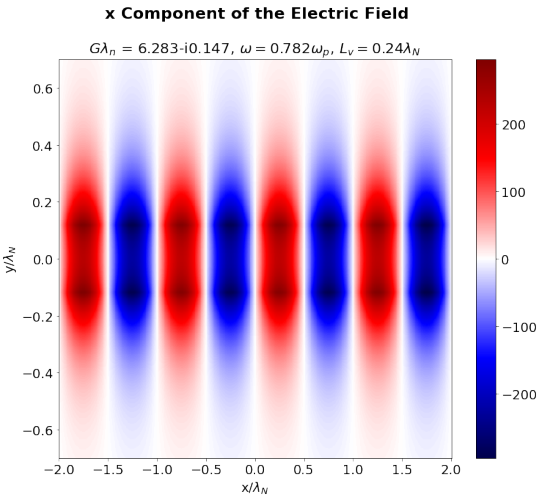

(a) Normalized x-component of the induced electric field.

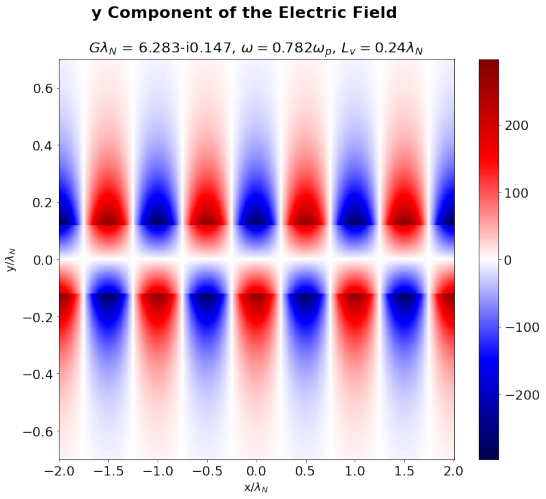

(b) Normalized y-component of the induced electric field.

Figure 5.7: Figures (a) and (b) show the x and y components of the induced electric field of a cavity SP excited resonantly via a grating coupler respectively. The components are given by Eqs. (4.49)-(4.52), where $E_{\text{ext}}\hat{x}$ is the external electric field which is the source of excitation. The field is normalized to the external field and the perturbative parameter as $E_{m/v}(x,y)/(E_{\text{ext}}h/\lambda_N)$. The coordinates are normalized to the grating period length λ_N.

5.3. Lengths scales, energy gains and their analysis.

Considering particles injected with a relatively small initial energy, then the final energy with which particles emerge from the accelerator is given in terms of the speed of the surface plasmon ω/Q_f, where ω is the SP frequency and Q_f is the wavevector at x_f, the position where particles are shoot out from the channel. Then the energy gain is approximately equal to

$$K = \frac{m}{2}\left(\frac{\omega}{Q_f}\right)^2. \tag{5.1}$$

We could fix the desired kinetic energy, which for our approximations should lie within the non-relativistic regime, and obtain the wavevector Q_f at exit, and the corresponding channel's aperture

$$L_f = \sqrt{\frac{2K}{m}}\frac{QL}{\omega}, \tag{5.2}$$

from which $L_f \propto \sqrt{K/m}/\omega$, where we substituted $Q_f = QL/L_f$. As K is at most the rest energy of the accelerated particle, with mass m, and with proportionality constant $QL = 1.5 = 3/2$,

$$\begin{aligned} K = \frac{m}{2}\left(\frac{\omega}{Q_f}\right)^2 &< mc^2, \\ \frac{1}{2}\left(\frac{\omega L_f}{1.5}\right)^2 &< c^2, \end{aligned} \tag{5.3}$$

from where we obtain

$$\begin{aligned} (\omega L_f)^2 &< 9c^2/2 \\ L_f &< \frac{3}{\sqrt{2}}\frac{\hbar c}{\hbar\omega} = \frac{3}{\sqrt{2}}\frac{0.197}{\hbar\omega}\text{eV}\,\mu\text{m}, \end{aligned} \tag{5.4}$$

in terms of the SP energy. For metals with plasma frequency around the UV regime $\hbar\omega \sim 10$ eV, the aperture to reach relativistic energies would be $L_f \sim 40$ nm.

To analyze the horizontal length x_f of the channel we first calculate the kinetic energy gained by our nominal particle interacting with the SP electric field. The SP electric field decays inversely proportional to the square root of the separation between the interfaces, but for simplicity (see below) we take for now as constant along the axis channel and equal to the field at the injection point. Then, the energy given to a particle that has travelled a distance x_f is

$$K_{\text{const}} = F_{\text{const}} x_f. \tag{5.5}$$

Comparing it with Eq. (5.1), we estimate the distance travelled to acquire that energy K as

$$\begin{aligned} x_f &= \frac{K}{F_{\text{const}}} = \frac{m}{2}\frac{(\omega/Q_f)^2}{q|E_i|\cos\theta_i} \\ &= \frac{2(\omega L_f)^2}{9q|E_i|\cos\theta_i/m}, \end{aligned} \tag{5.6}$$

which is inversely proportional to the amplitude of the electric field. Though this result is obtained for a constant field it is of the same order of magnitude as that obtained for the actual SP field, whose field changes as $E_{sp} \propto 1/\sqrt{L(x)}$ from Eq. (4.32), and it allows a simpler qualitative description of the results. To prove this statement, we calculate the work done by the SP's electric field,

$$\begin{aligned} W &= \int_0^{x_f} qE_{sp}(x,t)dx = q\int_0^{x_f} |E_i|\sqrt{\frac{Q(x)}{Q_i}}\cos\theta_i\, dx \\ &= q|E_i|\sqrt{\frac{\ln\Lambda}{Q_i}}\cos\theta_i \int_0^{x_f} \frac{dx}{\sqrt{L(x)}}. \end{aligned} \tag{5.7}$$

Substituting $L(x)$ from Eq. (4.26),

$$W = q|E_i|\cos\theta_i \int_0^{x_f} \frac{\sqrt{L_i}dx}{\sqrt{\left(\frac{5}{2}\frac{1}{\xi^2}\text{Re}(e^{i\theta_i})\eta Q_i x + 1\right)^{2/5} L_i}}. \tag{5.8}$$

This expression may be simplified if written in terms of the coordinate of the vertex

$$x_v = -\frac{\xi^2}{\frac{5}{2}\eta\cos\theta_i}. \tag{5.9}$$

x_v, for which $L(x_v) = 0$, yielding

$$W = q|E_i|\cos\theta_i \int_0^{x_f} \frac{dx}{\left(1+\frac{x}{|x_v|}\right)^{1/5}} = q|E_i|\cos\theta_i |x_v| \int_1^{\rho_f} \frac{d\rho}{\rho^{1/5}}, \tag{5.10}$$

where we changed the integration variable to $\rho = (1 + x/|x_v|)$, $d\rho = dx/|x_v|$.

Susbtituting η from Eq. (4.29) we obtain

$$W = \frac{5}{4} q|E_i|\cos\theta_i\, |x_v| \left[\left(1+\frac{x_f}{|x_v|}\right)^{4/5} - 1\right]. \tag{5.11}$$

For $|x_v| \gg x_f$, i.e., if injection takes place far from the vertex, then we recover the simple estimate given by Eq. (5.6). In the opposite limit, $x_f \gg |x_v|$ our previous estimate for the work has to be multiplied by a factor, $(|x_v|/x_f)^{1/5}$, so to obtain the same energy, the channel has to be larger,

i.e. $x_f = x_{f\,\mathrm{const}}^{5/4}/|x_v|^{1/4}$. The reason is that the field decreases along the channel, as it gets wider and the SP moves faster. Nevertheless, given our approximations, the injection point cannot be too close to the vertex, so the correction $(|x_v|/x_{f\,\mathrm{const}})^{1/4}$ would typically be close to 1.

Now let's consider the electric field of an available pulsed laser with an average power of, say, 5 W, a repetition frequency of 1 kHz, with pulses of duration 200 fs with a waist at focus of 1 μm^2. The energy per pulse is $\mathcal{E} = P/f = 5$ mJ and thus, its instantaneous power is $P_{\mathrm{ins}} = \mathcal{E}/\tau = 2.5\times10^7$ W, with an associated intensity $I = \frac{P}{A} = 2.5\times10^{14}$ W/cm^2 $= 2.5\times10^{21}$ ergs/s cm^2. From the intensity we can obtain the electric field amplitude identifying

$$|E_{\mathrm{ext}}| = \sqrt{\frac{8\pi}{c}I}, \tag{5.12}$$

obtaining $|E_{\mathrm{ext}}| = 1.4\times10^6$ gr$^{1/2}$/s cm$^{1/2}$, corresponding in SI units to $|E_{\mathrm{ext}}| = 43$ G V/m. A proton with electric charge $q = e$ would feel a force $F = e|E_{\mathrm{ext}}| = 43$ GeV/m. A typical plasma frequency is $\hbar\omega \approx 10$ eV i.e. $\omega \approx 1.5\times10^{15}$ Hz. We rewrite Eq. (5.6) as

$$x_f = \frac{2\sqrt{2}}{9}\frac{mc^2(\hbar\omega L_f)^2}{\hbar^2c^2e|E_i|}, \tag{5.13}$$

where we introduced our choice $\theta_i = \pi/4$ and used $\cos\theta_i = 1/\sqrt{2}$. Using our estimate above, $L_f \approx 40$ nm, the rest energy of the proton $mc^2 = 1$ GeV, and the amplitude factor of the field $|E_i| \approx 4E_{\mathrm{ext}}$, we estimate a length of the order of $x_f \approx (1/129)$ m ≈ 7 mm, only a few millimeters, but orders of magnitude larger than the width of the cavity.

Through a larger SP mediated amplification of the field we could make the device shorter. On the other hand, use of a lower powered, more accesible laser will require a larger cavity. In any case, the cavity turned out to be of the order of centimeters, so it would seems we have succeeded in designed a miniature accelerator in the GeV energy range of the order of a few centimeters long. Unfortunately, this small distance turns out to be huge when compared with the decay length of surface plasmons.

Chapter 6

CONCLUSIONS AND OUTLOOK

We have *designed* a miniature particle accelerator based on the excitation of surface plasmons (SP's) along a varying-width channel with conducting walls, so that the SP's coaccelerate with the particles. We obtained analytical results for the width of the channel $L(x)$ in the non-retarded limit, assuming that the free wavelength of the electromagnetic wave that excites the system mode is much larger than the system's plasmon's wavelength.

We further assumed that the change of the separation between the metallic interfaces is very gradual on the scale of the SP wavelength, and we obtained the field close to the center plane of the cavity between the plates. We treated the gradient of the separation as a small perturbative parameter. The electric potential turned out to be inversely proportional to the squared root of the local wavevector $Q(x)$ of the SP, and the electric field inversely proportional to the squared root of the interfaces separation $L(x)$. This may be easily understood through the conservation of energy: an SP wave going faster has a lower density of energy so that the total energy flux remains unchanged. Using our perturbative result along with the local dispersion relation for the symmetric SP mode, we obtained the equation of motion of charged particles immersed in the SP's electric field and we obtained the separation $L(x)$ by demanding that the SP move along the channel with the same acceleration as a chosen nominal particle with appropriate initial conditions. Co-acceleration means that at any time, the phase of the field at the position of the nominal particle is the same as the initial phase. This phase was chosen not to correspond to that for which the force is maximum, instead, we chose a phase such that particles that momentarily outruns the nominal particle would feel a smaller accelerating force, while those that are left behind would feel a larger force and would regain the nominal position; thus, longitudinal stability would be attained. Having chosen this nominal phase, we derived an analytical function that describes the channel's width $L(x)$ as a function of the position x along the channel. The function turns out to be surprisingly simple $L \propto (x - x_0)^{2/5}$, where x_0 is the injection position. This function fulfills the expected gradual change except very close to the vertex position x_v, where $L \approx 0$. From the width and the local dispersion relation functions, we obtained the local wavevector, whose spatial integral yields the wave's phase $\theta(x, t)$ that depends on the position x along the channel and the time t.

Having the previous results we studied the system's longitudinal stability, as shown in Figs. 5.2, 5.3, 5.5, and 5.4. We injected particles with different initial positions and velocities with respect to the nominal particle, and integrated the equations of motion, finding that for a wide range of initial conditions the particles are persistently accelerated, oscillating around the nominal particle. Persistent accelerations were obtained for particles with initial velocities up to five times the nominal initial velocity and initial positions up to three times the SP's wavelength away from the nominal initial position. Thus, we conclude that our proposed configuration is longitudinally stable and seems a sensible approach to steadily accelerate charged particles. An analysis of the transverse stability, by injecting particles with different velocities in the direction normal to the channel is pending. Our results were presented using properly normalized quantities, so that they

may be easily scaled for specific field amplitudes and energy gains.

Then we studied the excitation of the channel's normal mode. To that end we proposed generating SP's at the end of the channel by coupling incoming light to the normal mode providing the required momentum through a grating. Here we took advantage of the negative dispersion of the plasmon. We assumed a low angle coupler and we used a perturbative Rayleigh expansion to get the amplitude of the induced field in terms the exciting field and geometrical parameters. We considered a finite grating and set restrictions on their length in order to evaluate analytically the Fourier transform of the induced field using Cauchy's theorem. We considered a length for the grating coupler of a few times the grating's wavelength. The amplification of the field is shown in Figs. 5.7. Having studied an excitation method and estimating the field produced by available lasers we were able to compute the field induced within the channel and use it to find the other relevant accelerator parameters.

To estimate the size of our device, we used values within the range of our approximations to set an upper bound on the gained energy. Using the desired energy and the excitation field we were able to obtain definite values for our geometric parameters.

We assumed the initial kinetic energy is negligible and the final energy is bounded but close to the rest energy of the non-relativistic accelerated particle. We wrote the energy gained by the nominal particle in terms of the SP's phase velocity, and thus, in terms of its frequency and wavevector, which depends on the channel's width, and solved the channel's width which turned to be inversely proportional to the plasmon frequency. The length of the channel was estimated by equating the work done on the charged particle by the SP's electric field with the desired energy. The resulting length of the channel is nearly inversely proportional to the electric field amplitude, as could have been expected. Using a field with constant amplitude equal to the value at the injection point instead of the actual position dependent field along the channel yields a simple lower bound to the length of the device, as the actual field decreases as the particle advances.

Using silver, which is a suitable metal for plasmonic phenomena, modelling it through the Drude model, neglecting the contribution to its response from relatively bound electrons, and considering the acceleration of protons with an energy gain up to their rest energy, the width resulted of the order of tens of nanometers. Estimating the external field as that from a pulsed laser with a peak intensity in the range of 10^{14} W/cm^2 we obtained a length of approximately 0.7cm. *¡Fabulous!* A nanostructure to accelerate charged particles to high energies of the order of GeV's just a few centimeters long.

Not so fast. Even assuming that drilling a centimeter long nanohole in a metal isn't problematic, the SP's propagation lengths in ordinary metals are approximately one thousand times smaller than one centimeter. Our SP mode won't reach the injection point of our cavity to accelerate the injected particles, or if the field is somehow excited at the injection point, it would die out before the particle reaches a sizable energy. Nevertheless the inconvenient relatively small SP's propagation length doesn't invalidate our proposed acceleration mechanism. Rather, it encourages us to search for alternative materials with SP's or similar modes whose frequencies are smaller to overcome the difficulty of drilling a nanochannel, whose wavelengths are bigger and whose dissipation is smaller, so they can travel all along the channel. For example, doped semiconductors have frequencies in the THz regime and propagation lengths one or two orders of magnitude bigger than in silver and gold [44]. Another alternative is to employ *Spoof Surface Plasmons*, superficial modes in metamaterials whose characteristics are similar to SP's in noble metals but with frequencies in the THz and microwave regimes and with propagation lengths larger than SP's in semiconductors [45]. Aditionally, their properties are tunable through geometrical changes in the metamaterial composition and geometry.

Our results also require a reformulation that includes retardation to allow accelerating particles up to the relativistic regime. It is also necessary to analyse the feasibility of fabricating the resulting structures and of evaluating the limits on the field in order to avoid damage due to intense laser irradiation. This will be the subject of further work.

Appendix A

APPENDIX I

This Appendix presents the full derivation and approximations taken to get the potential of the cavity having a variable separation distance between the interfaces along the x axis.

The electrostatic potential within a cavity formed by two seminfinite parallel plates separated a distance L along the y direction was obtained as

$$\Phi(x,y,t) = (\phi_+ e^{Qy} + \phi_- e^{-Qy}) e^{i(Qx-\omega t)}, \qquad \text{(Rep. Eq. 4.4)}$$

in Sec. 4.1, where $\phi_\pm$ are constants, and are equal for the symmetric mode. We use the solution given by Eq. 4.4 for the symmetric mode but with a position dependent amplitude $\phi_s(x)$ slowly varying along x as an *ansatz*. We neglect the y dependence of $\phi_s$since we limit ourselves to the center of the channel $y = 0$ where the first derivative in y of ϕ is zero and the other terms remainig in the differential equation are of second order in y.

Furthermore, we replace the x dependent phase $\pm Qx$ by the total accumulated phase $\pm \int^x dx' Q(x')$ with $Q(x)$ the local wavevector at position x. We substitute this *ansatz* in Laplace equation

$$\nabla^2\Phi(x,y,t) = \partial_y^2(\phi_s(x) e^{i\int^x Q(x')dx'} \cosh(Q(x)y)) + \partial_x^2(\phi_s(x) e^{i\int^x Q(x')dx'} \cosh(Q(x)y)). \quad \text{(A.1)}$$

We develop the second partial derivative in x

$$\begin{aligned}
\partial_x^2\Phi(x,y,t) = \partial_x \Big\{ e^{i\int^x Q(x')dx'} \Big[&(\partial_x\phi_s(x)) \cosh(Q(x)y) + \phi_s(x)(iQ(x)) \cosh(Q(x)y) \\
&+ \phi_s(x) \sinh(Q(x)y) y (\partial_x Q(x)) \Big] \Big\} \\
= e^{i\int^x Q(x')dx'} \Big[&(\partial_x^2\phi_s(x)) \cosh(Q(x)y) + 2i(\partial_x\phi_s(x))Q(x) \cosh(Q(x)y) \\
&+ (\partial_x\phi_s(x))(\partial_x Q(x)) y \sinh(Q(x)y) + i\phi_s(x)(\partial_x Q(x)) \cosh(Q(x)y) \\
&- \phi_s(x)(Q(x))^2 \cosh(Q(x)y) + i\phi_s(x)Q(x)y \sinh(Q(x)y)(\partial_x Q(x)) \\
&+ (\partial_x\phi_s(x))(\partial_x Q(x)) y \sinh(Q(x)y) + i\phi_s(x)(\partial_x Q(x))Q(x)y \sinh(Q(x)y) \\
&+ \phi_s(x)(\partial_x^2 Q(x)) y \sinh(Q(x)y) + \phi_s(x)(\partial_x Q(x))^2 y^2 \cosh(Q(x)y) \Big] \\
= e^{i\int^x Q(x')dx'} &(\partial_x^2\phi_s(x))(\cosh(Q(x)y)) + \partial_x\phi_s(x) \Big[2iQ(x) \cosh(Q(x)y) \\
&+ 2y(\partial_x Q(x)) \sinh(Q(x)y) \Big] + \phi_s(x) \Big[-(Q(x))^2 \cosh(Q(x)y) \\
&+ (\partial_x Q(x)) \Big[i2Q(x)y \sinh(Q(x)y) + i\cosh(Q(x)y) + y^2(\partial_x Q(x)) \cosh(Q(x)y) \Big] \Big].
\end{aligned}$$

Repeat 4.10a

Similarly, we develop the second partial derivative in y,

$$\begin{aligned}\partial_y^2\Phi(x,y,t) =&\partial_y\left[\phi_s(x)e^{i\int^x Q(x')dx'}Q(x)\sinh\left(Q(x)y\right)\right]\\ =&\left[\phi_s(x)e^{i\int^x Q(x')dx'}(Q(x))^2\cosh\left(Q(x)y\right)\right].\end{aligned} \qquad \text{Repeat 4.10b}$$

Assuming the changes along x of the separation $L(x)$ between the plates are gradual, the changes of the wavevector $Q(x)$ and of the amplitude $\phi_s(x)$ also be gradual. Then the nonlinear and second derivative terms in x, such as $(\partial_x Q(x))^2$ and $(\partial_x\phi(x))(\partial_x Q(x))$ may be neglected with respect to the other terms. Thus, the Laplacian is approximately given by

$$\begin{aligned}\nabla^2\Phi(x,y,t) = \partial_y^2\Phi(x,y,t) + \partial_x^2\Phi(x,y,t),\\ = \partial_x\phi_s(x)\Big[2iQ(x)\cosh\left(Q(x)y\right)\Big] + \phi_s(x)\partial_x Q(x)\Big[2iQ(x)y\sinh\left(Q(x)y\right) + i\cosh(Q(x)y)\Big].\end{aligned} \qquad \text{Repeat 4.11}$$

Restricting ourselves to the middle of the channel, $y\to 0$, substituting the terms $iy\sinh\left(Q(x)y\right)\to 0$ and $\cosh(Q(x)y)\to 1$, we get a simplified equation

$$2(\partial_x\phi_s(x))Q(x) + \phi_s(x)(\partial_x Q(x)) = 0, \qquad \text{Repeat 4.12}$$

which is a logarithmic differential equation with solution

$$\begin{aligned}\ln\frac{\phi_s(x)}{\phi_s(x_0)} =& -\ln\left(\frac{Q(x)}{Q(x_0)}\right)^{1/2},\\ \phi_s(x) =&\sqrt{\frac{Q(x_0)}{Q(x)}}\phi_0,\end{aligned} \qquad (A.2)$$

giving a potential in the middle $y\to 0$ of the channel equal to

$$\Phi(x,y=0,t) = \sqrt{\frac{Q(x_0)}{Q(x)}}\phi_0 e^{i(\int^x Q(x')dx'-\omega t)}. \qquad \text{Repeat 4.14}$$

Appendix B

APPENDIX II

This Appendix presents the theory of the approaches that were abandoned, but that were preliminary work that helped me to understand the relevant criteria on the mechanism presented for the acceleration of SP.

The studied surface waves were those that propagate along the interfaces between a dielectric (or vacuum) and dielectric-dielectric or metal-dielectric superlattices. Since we employ dielectric media, we present the *Lorentz* dielectric media model. Then we derive Fresnel reflection coefficients of light impinging on flat interfaces between two different media and use them to obtain the dispersion relation of the surface waves from the reflection pole. To express the reflection coefficients in a compact manner, we introduce the surface impedance, we write it in terms of wavevector of light impinging on the surface and use it to obtain the reflection amplitude.

We studied surface waves of laminar media using the transfer matrix formalism. We applied it to periodically layered media employing Bloch's theorem to find the lattice eigenmodes and obtain the surface impedance of periodic dielectric-dielectric lattices. We then use the superface impedance to determine the pole of the reflection coefficient which yields the surface wave dispersion relation. The surface waves that propagate at the interface between the dielectric-dielectric superlattice are known as *Tamm Waves*.

To study the surface waves on the interface of metallodielectric superlattices whose period is composed of two films of different media, metal and dielectric, we apply the effective media approximation and find its effective dielectric function. The effective medium turns out to be anisotropic. Hence we present the theory of the propagation of light through anisotropic media to obtain the wavevectors which we use to get the impedance and from it, the pole of the reflection amplitude and the dispersion relation of the surface waves.

B.1. Dielectric Media

We model a dielectric medium as an arrangement of regularly positioned atoms with bound electrons which are displaced from their equilibrium positions giving rise to a polarization that is described by the electric susceptibility of the medium. An ideal dielectric has zero electric conductivity and therefore only exhibits polarization due to the motion of the bound charges in atoms. There are classical models to understand the dependence on the frequency of the permittivity. One of the main ones is the *Debye Model*, which applies to polar dielectrics, when molecules have permanent electric moments. The model considers that when switching off the external field, the polarization vector will exponentially decay due to thermalization, $\boldsymbol{P}(t) = \boldsymbol{P}_o e^{-t/T}$, where the relaxation time T depends on the material properties and temperature. The common form of the known result of the dielectric function is $\epsilon(\omega) = 1 + \frac{\epsilon_s - 1}{1 + i\omega T}$, where ϵ_s is the permittivity at zero frequency. The second main model, *Lorentz Model*, is applied to media whose molecules acquire a dipole only when interacting with external fields, and considers oscillations of an electron near its

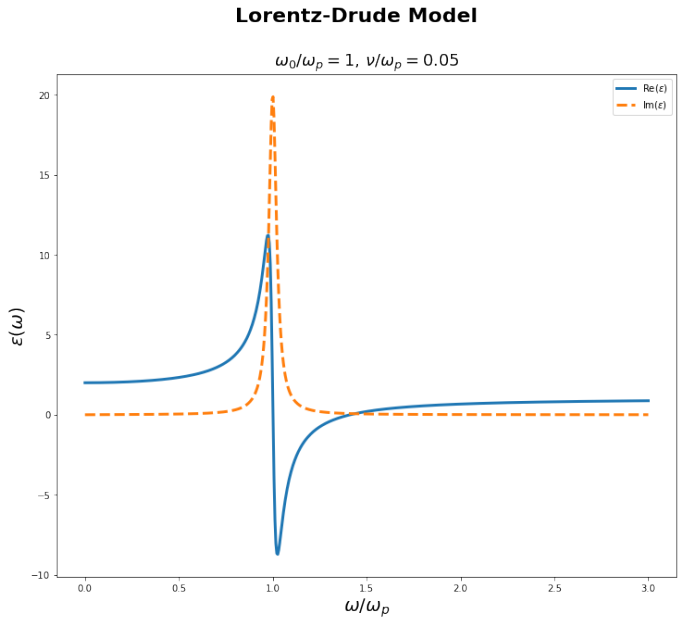

Figure B.1: Generic frequency dependence of the dielectric function derived using the Lorentz model of dielectric media.

equilibrium point under the influence of an external oscillating electric field $\boldsymbol{E}$. The model considers that the motion of charge carriers is dictated by the Lorentz force $\boldsymbol{F} = q\boldsymbol{E}$, a harmonic restoring force $\boldsymbol{F}_r = -\kappa \boldsymbol{r}$ where $\boldsymbol{r}$ is the displacement from equilibrium, and a friction force $\boldsymbol{F}_f = -\Gamma \frac{d\boldsymbol{r}}{dt}$. Then the equation of motion for electrons is

$$m\frac{d^2\boldsymbol{r}}{dt^2} + \Gamma\frac{d\boldsymbol{r}}{dt} + \kappa\boldsymbol{r} = -e\boldsymbol{E}. \tag{B.1}$$

Assumming a time-harmonic dependence, the solution is

$$\boldsymbol{r} = \frac{-e/m}{\omega_0^2 - \omega^2 + i\omega\nu}\boldsymbol{E}, \tag{B.2}$$

where $\omega_0^2 = \kappa/m$ is the resonant frequency and $\nu = \Gamma/m$ is the inverse of the damping time. The contribution to the dipole moment is $\boldsymbol{p} = -e\boldsymbol{r}$ and considering n electrons per unit volume, we have a polarization $\boldsymbol{P} = n\boldsymbol{p}$. Since the displacement vector is given by $\boldsymbol{D} = \boldsymbol{E} + 4\pi\boldsymbol{P} = \epsilon\boldsymbol{E}$, the permittivity results

$$\epsilon(\omega) = \left(1 + \frac{\omega_p^2}{\omega_0^2 - \omega^2 + i\omega\nu}\right), \tag{B.3}$$

where $\omega_p^2 = \frac{4\pi n e^2}{m}$. The frequencies ω_p and ω_0 determine the optical properties of the media such as transparency, opacity, or resonances as a function of the field frequency ω. The general behaviour of a dielectric described by Lorentz model is as shown in the Fig. B.1

B.2. Reflection on Flat Interfaces

First, we introduce the two linear polarization of light, *TE* and *TM* where electric and magnetic fields are perpendicular to the incidence plane respectively, and the definition of surface impedance in terms of wavevectors. Then we derive the Fresnel reflection coefficient written in terms of impedances, which simplifies the resulting expressions.

Transverse Electric Polarization

Consider two different media separated by a flat interface. Consider a plane wave with wavevector $\boldsymbol{k}$. The plane that contains $\boldsymbol{k}$ and the normal to the interface is the *plane of incidence*. If the electric field is normal to the plane of incidence, the wave is said to have *transverse electric polarization (TE, or s)*. For example, assuming that the interface that delimits two media lies on the xy plane and that the plane of incidence is yz, as shown in Fig. B.2, s polarized waves have their electric field along x.

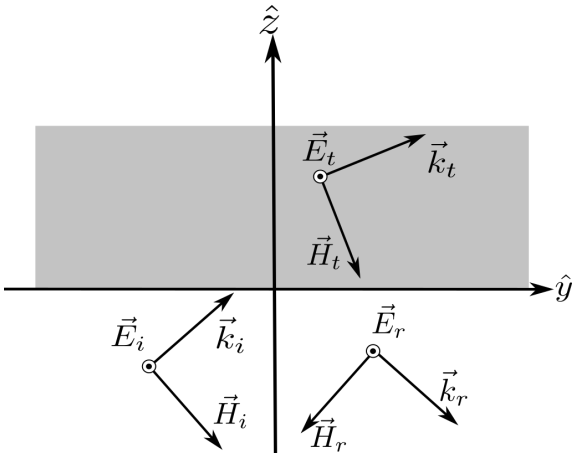

Figure B.2: An s or TE-polarized plane wave impinging on the boundary between two media has its electric field $\boldsymbol{E}$ along the perpendicular direction to the plane of incidence. The plane of incidence is defined by the wavevector $\boldsymbol{k}$ and the normal to the surface. The wave's magnetic field $\boldsymbol{H}$ lies on the plane of incidence. The transmitted and reflected s-polarized waves are also indicated.

Transverse Magnetic Polarization

Plane waves whose magnetic field is along the normal to the plane of incidence are said to have *transverse magnetic polarization, (TM, or p)*. The vector representation is shown in Fig. B.3, where yz is the plane of incidence and x the direction of the magnetic field.

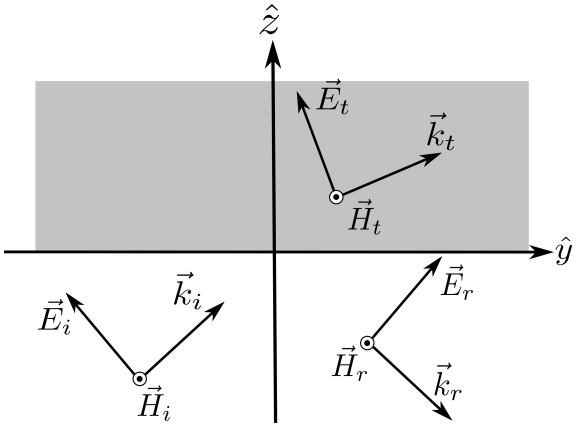

Figure B.3: A p-polarized plane wave impinging on the boundary between two media has its magnetic field $\boldsymbol{H}$ along the perpendicular direction to the plane of incidence and its electric field $\boldsymbol{E}$ liying on the plane of incidence. The reflected and transmitted fields are indicated.

Surface Impedance

The polarization of an electromagnetic plane wave tell us the direction of the fields and propagation. Using Faraday and Ampère-Maxwell equations we can find the different field components in terms of the wavevector components and frequency.

The *surface impedance* is defined as the quotient between parallel components of the fields,

$$Z = \frac{E_{\parallel}}{H_{\parallel}}. \tag{B.4}$$

The surface impedances for plane waves are

$$\begin{aligned} Z_{\alpha}^{s} &= \frac{1}{k_{\perp}^{\alpha}} \left(\frac{\omega}{c}\right), \\ Z_{\alpha}^{p} &= \frac{k_{\perp}^{\alpha}}{\epsilon_{\alpha}} \left(\frac{c}{\omega}\right), \end{aligned} \tag{B.5}$$

for each polarization, where $k_{\perp}^{\alpha}$ is the component of the wavevector normal to the interface within medium α. Notice that the surface impedance for a reflected wave has the opposite sign to that of the corresponding incident wave.

B.2.1. Fresnel Reflection Coefficients

As electromagnetic waves propagates across the interface between two different media, light experiments a backward scattering, a reflection. The reflection amplitude of a wave is defined as the quotient between the amplitude of the reflected and incident fields. Depending on the wave's polarization, the definition of the reflection amplitude is conveniently chosen in terms of either the electric or magnetic fields, whichever field is perpendicular to the plane of incidence, as

$$r^{s} = \frac{E^{r}}{E^{i}}, \tag{B.6a}$$

$$r^{p} = \frac{H^{r}}{H^{i}}. \tag{B.6b}$$

The continuity of the field projections onto the interface, which we take as the xy plane, is given by

$$\left\{ \begin{aligned} E_{x}^{t} &= (1 + r^{s}) E_{x}^{i}, \\ H_{y}^{t} &= (1 - r^{s}) E_{x}^{i} / Z_{i}^{s}, \end{aligned} \right\} \tag{B.7}$$

for s polarization, and

$$\left\{ \begin{aligned} H_{x}^{t} &= (1 + r^{p}) H_{x}^{i}, \\ E_{y}^{t} &= -(1 - r^{p}) H_{x}^{i} Z_{i}^{p} \end{aligned} \right\} \tag{B.8}$$

for p polarization. Here, the superscript t denotes transmited and i incident fields. Eqs. (B.7), (B.8) and the definition of the surface impedance Eq. (B.4), let us relate the impedances with the reflection coefficients as,

$$Z_{t}^{s} = \frac{(1 + r^{s})}{(1 - r^{s})} Z_{i}^{s}, \tag{B.9a}$$

$$Z_{t}^{p} = \frac{(1 - r^{p})}{(1 + r^{p})} Z_{i}^{p}, \tag{B.9b}$$

where Z_i and Z_t are the surface impedances of the media from which the wave impinges on the interface and the media into which it is transmitted, respectively. We obtain, thus, the reflection

amplitude in terms of the surface impedances of the media involved for the two different linear polarizations,

$$r^s = \frac{(Z_i^s - Z_t^s)}{(Z_i^s + Z_t^s)}, \tag{B.10a}$$

and

$$r^p = \frac{(Z_t^p - Z_i^p)}{(Z_t^p + Z_i^p)}. \tag{B.10b}$$

From the poles of these reflection coefficients we get the normal modes of an interface implicitly as

$$(Z_t^\zeta + Z_i^\zeta) = 0, \tag{B.11}$$

where $\zeta = \{\text{s,p}\}$ is the wave polarization.

B.3. Propagation of Plane Electromagnetic Waves Through Laminar Structures

We described the reflection process that electromagnetic waves suffer when passing through two different media separated by a flat interface. Using these results we study the propagation of electromagnetic waves through multiple media delimited by flat surfaces, generalizing the light propagation through n different media films via the transfer matrix method. Then we develop the specific case where the media is made of a periodic array of two films of different media using the transfer matrix formalism along with Bloch's theorem, and we find the surface impedance of a periodic lattice. To study the metallodielectric lattice we develop an effective medium approximation, where analytical calculations can be easily performed. Lastly, since the effective media results to be anisotropic, we present the theory of propagation of electromagnetic waves in anisotropic media in order to obtain the perpendicular wavevector in terms of the dielectric response and obtain the reflection pole, from which we obtain the dispersion relation of the surface waves.

B.3.1. Transfer Matrix

Let us consider the electromagnetic field within a film bounded by two flat parallel interfaces as the sum of the electromagnetic fields of two sinusoidal waves $E = E_+ + E_-$, a rising wave with amplitude $|E_+|$ and a wave going down with amplitude $|E_-|$. Using the impedance definition (Eq. (B.4)) we can write the projections of the magnetic and electric fields upon the interfaces in matrix form as

$$\begin{pmatrix} E_\parallel^s(z) \\ H_\parallel^s(z) \end{pmatrix} = \begin{pmatrix} 1 & 1 \\ 1/Z^s & -1/Z^s \end{pmatrix} \begin{pmatrix} E_+^s e^{ik_\perp z} \\ E_-^s e^{-ik_\perp z} \end{pmatrix} \equiv \boldsymbol{N}^s \begin{pmatrix} E_+^s e^{ik_\perp z} \\ E_-^s e^{-ik_\perp z} \end{pmatrix} \tag{B.12}$$

for s polarization and

$$\begin{pmatrix} E_\parallel^p(z) \\ H_\parallel^p(z) \end{pmatrix} = \begin{pmatrix} -Z^p & Z^p \\ 1 & 1 \end{pmatrix} \begin{pmatrix} H_+^p e^{ik_\perp z} \\ H_-^p e^{-ik_\perp z} \end{pmatrix} \equiv \boldsymbol{N}^p \begin{pmatrix} H_+^p e^{ik_\perp z} \\ H_-^p e^{-ik_\perp z} \end{pmatrix}, \tag{B.13}$$

for p polarization. Here we used that the sign of the surface impedance for downward moving waves is the opposite as that for upwards moving waves, as it depends on the direction of the perpendicular component of the wavevector. Now let's consider the films width is d with its interfaces placed in $z = z_-$ and $z = z_+ = z_- + d$. The rising field and the ones going down inside the film differ from one interface to another by a phase, such change can be written as a linear transformation

$$\begin{pmatrix} E_+ e^{ik_\perp z_+} \\ E_- e^{-ik_\perp z_+} \end{pmatrix} = \begin{pmatrix} e^{ik_\perp d} & 0 \\ 0 & e^{-ik_\perp d} \end{pmatrix} \begin{pmatrix} E_+ e^{ik_\perp z_-} \\ E_- e^{-ik_\perp z_-} \end{pmatrix} = \boldsymbol{D} \begin{pmatrix} E_+ e^{ik_\perp z_-} \\ E_- e^{-ik_\perp z_-} \end{pmatrix}, \tag{B.14}$$

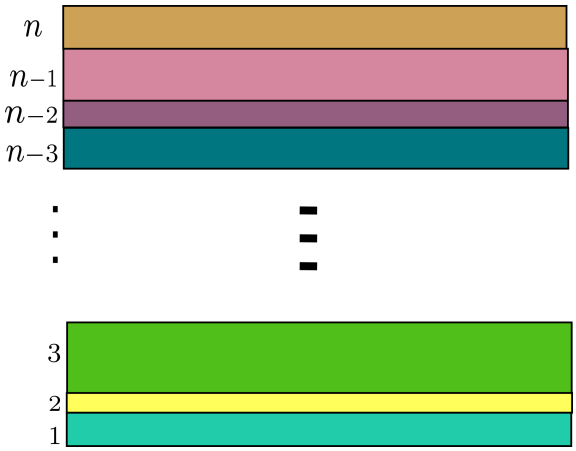

Figure B.4: Structure composed of n films of different media characterized by their response functions, ϵ_n and Z_n.

where we identified the diagonal matrix

$$\boldsymbol{D} = \begin{pmatrix} e^{ik_\perp d} & 0 \\ 0 & e^{-ik_\perp d} \end{pmatrix}. \tag{B.15}$$

Thus, the parallel fields at interface z_+, may be written in terms of the field at the opposite interface z_- across film's width d, as

$$\begin{pmatrix} E_\parallel^\zeta(z_+) \\ H_\parallel^\zeta(z_+) \end{pmatrix} = \boldsymbol{m}^\zeta \begin{pmatrix} E_\parallel^\zeta(z_-) \\ H_\parallel^\zeta(z_-) \end{pmatrix}, \tag{B.16}$$

where, after some algebra, using the fields written as in Eqs. (B.12), (B.13), and that $z_+ - z_- = d$, we find the transfer matrix $\boldsymbol{m}^\zeta$ to be

$$\boldsymbol{m}^\zeta = \left(\boldsymbol{N}^\zeta \boldsymbol{D} (\boldsymbol{N}^\zeta)^{-1}\right). \tag{B.17}$$

The matrix product yields,

$$\boldsymbol{m}^\zeta = \begin{pmatrix} \cos(k_\perp d) & iZ^\zeta \sin(k_\perp d) \\ i\frac{\sin(k_\perp d)}{Z^\zeta} & \cos(k_\perp d) \end{pmatrix} \tag{B.18}$$

which has the same form for both wave polarizations, but with different values for the surface impedance.

Generalization to n Films

Let us consider n films of different materials with characteristic response functions ϵ_n and Z_n, as shown in Fig. B.4. The fields at the interfaces of every film are related via a transfer matrix as Eq. (B.16) and, as the parallel projections of the electric and magnetic fields are continuous at each interface, the fields between interfaces i and j of different films are similarly related via

$$\begin{pmatrix} E(z_i) \\ H(z_i) \end{pmatrix} = \boldsymbol{M} \begin{pmatrix} E(z_j) \\ H(z_j) \end{pmatrix}, \tag{B.19}$$

where

$$\boldsymbol{M} = \prod_n m_n, \tag{B.20}$$

where m_n is the transfer matrix of the $n-th$ film and the product is over all intervening films.

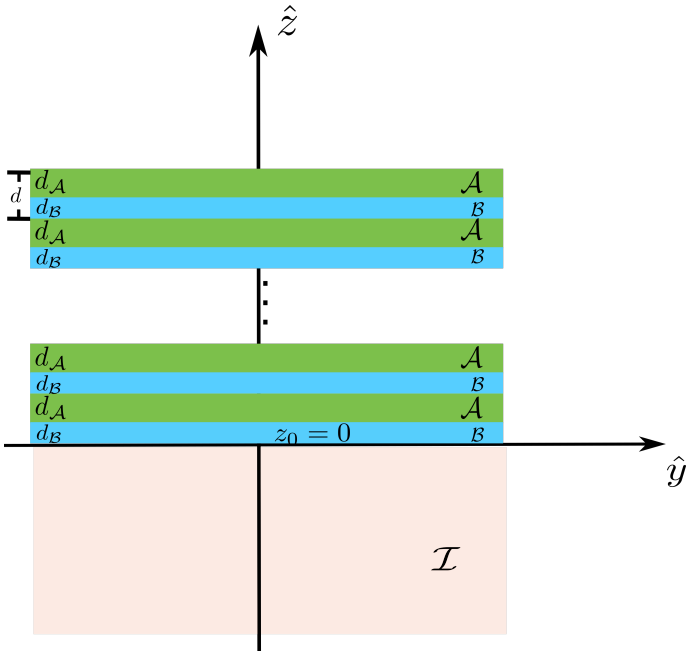

Figure B.5: System composed of a semiinfinite homogeneous medium $\mathcal{I}$ and a semiinfinite periodic superlattice $\mathcal{P}$ composed of two films of different materials A and B with widths d_A and d_B. The periodicity is along $\hat{z}$.

Periodic Structures

Consider two different systems, an homogeneous medium $\mathcal{I}$ that occupies the space $z < 0$ and a composite medium $\mathcal{P}$ periodically structured along the z direction, perpendicular to the interfaces, composed of two different materials, A and B with widths d_A and d_B respectively occupying the semi-space $z > 0$ with period $d = d_A + d_B$ as illustrated in Fig. B.5. Within the periodic superlattice the propagating modes of the system can be written as a superposition of Bloch modes, which acquire a phase $e^{i\beta d}$ after traveling a period, where β is the Bloch vector. We can relate the fields across a period through

$$\begin{pmatrix} E_{\parallel}^{\zeta}(z_i + d) \\ H_{\parallel}^{\zeta}(z_i + d) \end{pmatrix} = \boldsymbol{M} \begin{pmatrix} E_{\parallel}^{\zeta}(z_i)) \\ H_{\parallel}^{\zeta}(z_i) \end{pmatrix} = e^{i\beta_{\zeta} d} \begin{pmatrix} E_{\parallel}^{\zeta}(z_i)) \\ H_{\parallel}^{\zeta}(z_i) \end{pmatrix}, \tag{B.21}$$

where $\boldsymbol{M}$ is the transfer matrix of a single period. This is an eigenvalue problem with eigenequation

$$\left(\boldsymbol{M}^{\zeta} - \Lambda^{\zeta}\right) \begin{pmatrix} E_{\parallel}^{\zeta}(z_i) \\ H_{\parallel}^{\zeta}(z_i) \end{pmatrix} = 0, \tag{B.22}$$

in which $\Lambda^{\zeta} = e^{i\beta_{\zeta} d}$ is the eigenvalue of $\boldsymbol{M}^{\zeta}$. The characteristic equation is simplified to

$$\cos(\beta_{\zeta} d) = \frac{1}{2}\mathrm{Tr}(\mathrm{M}^{\zeta}), \tag{B.23}$$

since $\det M^{\zeta} = 1$. That $\det M^{\zeta} = 1$ means that the two eigenvalues of $\boldsymbol{M}$ are reciprocal to each other; if one corrersponds to an upward moving Bloch wave, the other would correspond to the downward moving Bloch wave. Even with a negligibly small dissipation, one of the modes will obey $|\Lambda^{\zeta}| < 1$, corresponding to a field that decays when going upwards $z \to \infty$; then, the other eigenvalue is $1/\Lambda^{\zeta}$ with magnitude > 1, and it presents decay when going downwards $z \to -\infty$.

Notice in the eigenequation Eq. (B.22) that the Bloch vector must be real for infinite systems to avoid divergences in $z = \pm\infty$. However, in semiinfinite systems, complex values of the Bloch vector are allowed as long as the only chosen eigenvalue corresponds to a mode that decays when $z \to \pm\infty$.

From the eigenequation shown in Eq. (B.22), we obtain the eigenvector corresponding to the eigenvalue $\Lambda_\zeta = e^{i\beta_\zeta d}$ of the waves in the periodic structure,

$$\begin{pmatrix} E_\parallel^\zeta(z+d) \\ H_\parallel^\zeta(z+d) \end{pmatrix}_{z>z_0} = e^{i\beta_\zeta d} \begin{pmatrix} 1 \\ \frac{(e^{i\beta_\zeta d} - M_{11}^\zeta)}{M_{12}^\zeta} \end{pmatrix}, \tag{B.24}$$

from which the impedance of the periodic media $\mathcal{P}$ is obtained

$$Z_{\mathcal{P}}^\zeta = \frac{M_{12}^\zeta}{(e^{i\beta_\zeta d} - M_{11}^\zeta)}. \tag{B.25}$$

From this impedance, the reflection amplitude and the normal modes of the homogeneous-periodic interface may be calculated using Eqs. (B.10a), (B.10b), and (B.11).

B.3.2. Effective Medium Approximation

Now let us consider two media, an homogeneous $\mathcal{I}$ media, and a periodic superlattice $\mathcal{E}$ made up with two alternated films A and B with widths d_A and d_B with dielectric functions ϵ_A and ϵ_B as in the previous subsection and as illustrated in Fig. B.6, but where the films' widths are very small, so that $d_A, d_B \ll \lambda_0$, with λ_0 being the free space wavelength. The superlattice may then be described by an effective medium approximation. This approximation describes a composite medium in terms of an effective permittivity and susceptibility of the whole structure. These properties depend on the composition and geometry of the components.

Maxwell's equations imply the continuity of certain *microscopic* fields projections at the boundaries inside the lattice. As we are assuming that d_a and d_b are very small compared to the wavelength, we may assume that within a single film the change of any component of any field is negligible. On one hand, the perpendicular component of the electric field and the parallel component of the displacement are discontinuous at the interfaces, with jumps when changing from one film to the next one another, as Fig. B.7 illustrates. On the other hand, due to continuity of the parallel component of the electric field and of the perpendicular component of the displacement field on each interface within the super lattice, these are practically constants along the super lattice for distances smaller than the wavelength, i.e. for $z' - z < \lambda_0$

$$\begin{aligned} \boldsymbol{E}_\parallel(z) &= \boldsymbol{E}_\parallel(z'), \\ D_\perp(z) &= D_\perp(z'), \end{aligned} \tag{B.26}$$

where z, z' are points inside the $\mathcal{E}$ system. Calculating the macroscopic fields $\boldsymbol{E}^M$ and $\boldsymbol{D}^M$, defined as the spatial average of the corresponding microscopic fields over a period, is trivial. The average of the components in Eq. (B.26) are themselves, $\boldsymbol{E}_\parallel(z) = \boldsymbol{E}_\parallel^M(z)$ and $D_\perp(z) = D_\perp^M(z)$. The parallel component of the macroscopic displacement field is calculated as

$$\begin{aligned} \boldsymbol{D}_\parallel^M(z) &= \langle \boldsymbol{D}_\parallel(z) \rangle \\ &= \langle \epsilon(z) \boldsymbol{E}_\parallel(z) \rangle \\ &= \langle \epsilon(z) \rangle \boldsymbol{E}_\parallel^M(z) \\ &\equiv \epsilon_\parallel^M \boldsymbol{E}_\parallel^M(z). \end{aligned} \tag{B.27}$$

Taking

$$\epsilon(z) = \begin{cases} \epsilon_a \ , & \text{within a-layers} \\ \epsilon_b \ , & \text{within b-layers,} \end{cases} \tag{B.28}$$

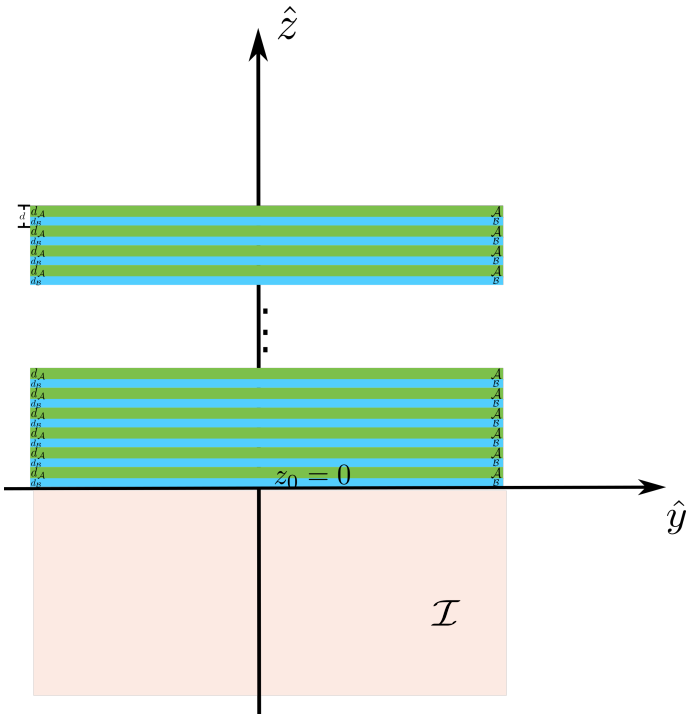

Figure B.6: Homogeneous media $\mathcal{I}$ next to a periodic super lattice $\mathcal{E}$ made up of thin films of different media A y B with widths d_A y d_B, and dielectric functions ϵ_A y ϵ_B. Given that the widths are assumed too small $d_A \to 0$ and $d_B \to 0$ the super lattice $\mathcal{E}$ is well described as an effective medium.

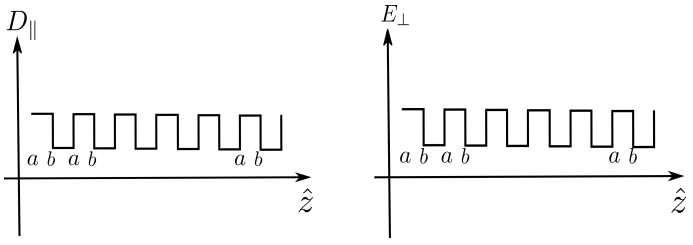

Figure B.7: Parallel component of the microscopic displacement (left) and perpendicular component of the microscopic electric field within a superlattice with a very small period. The microscopic fields are approximately constant within each film, but the normal components jump discontinuously at each interface.

the macroscopic response of the system in the direction parallel to the interfaces is

$$\begin{aligned} \epsilon_{\parallel}^{M} &= \langle \epsilon(z) \rangle \\ &= f_a \epsilon_a + f_b \epsilon_b \\ &= \frac{d_a}{d}\epsilon_a + \frac{d_b}{d}\epsilon_b, \end{aligned} \tag{B.29}$$

where we introduced the filling fractions $f_a = d_a/d$ and $f_b = d_b/d$. Similarly, we calculate the average of the perpendicular component of the electric field,

$$\begin{aligned} E_{\perp}^{M} &= \langle E_{\perp}(z) \rangle \\ &= \left\langle \frac{D_{\perp}(z)}{\epsilon(z)} \right\rangle \\ &= \left\langle \frac{1}{\epsilon(z)} \right\rangle D_{\perp}^{M} \\ &= \frac{1}{\epsilon_{\perp}^{M}} D_{\perp}^{M}, \end{aligned} \tag{B.30}$$

where we have to calculate the average over a period of the inverse of the macroscopic response of the system in the perpendicular direction,

$$\begin{aligned} \frac{1}{\epsilon_{\perp}^{M}} &= \left\langle \frac{1}{\boldsymbol{\epsilon}(z)} \right\rangle \\ &= \frac{f_a}{\epsilon_a} + \frac{f_b}{\epsilon_b} \\ &= \frac{d_a}{d}\frac{1}{\epsilon_a} + \frac{d_b}{d}\frac{1}{\epsilon_b}. \end{aligned} \tag{B.31}$$

Thus finally we obtain that the superlattice is characterized by an *effective* macroscopic anisotropic dielectric function

$$\boldsymbol{\epsilon} = \begin{pmatrix} \epsilon_{\parallel} & 0 \\ 0 & \epsilon_{\perp} \end{pmatrix} = \begin{pmatrix} \frac{d_a}{d}\epsilon_a + \frac{d_b}{d}\epsilon_b & 0 \\ 0 & \left(\frac{d_a}{d}\frac{1}{\epsilon_a} + \frac{d_b}{d}\frac{1}{\epsilon_b}\right)^{-1} \end{pmatrix}. \tag{B.32}$$

This development was done for a two component structure but can be extended for more components using the corresponding boundary conditions. We have obtained the effective response of the metallodielectric superlattice, which we use to obtain the reflection amplitude of light impigning from vacuum at the lattice interface.

Since we obtained an anisotropic effective media we study the propagation of light within anisotropic media to find the dispersion relations; we then calculate the reflection amplitude.

B.4. Propagation of Plane Electromagnetic Waves in Anisotropic Media

Consider a plane wave that propagates in the absence of external sources within a nonmagnetic homogeneous anisotropic medium with permittivity $\boldsymbol{\epsilon}(\omega, \boldsymbol{k})$ and permeability $\mu(\omega, \boldsymbol{k}) = 1$, with fields

$$\boldsymbol{E} = \boldsymbol{E}_0 e^{i(\boldsymbol{k}\cdot\boldsymbol{r} - \omega t)}, \tag{B.33a}$$

$$\boldsymbol{H} = \boldsymbol{H}_0 e^{i(\boldsymbol{k}\cdot\boldsymbol{r} - \omega t)}, \tag{B.33b}$$

where $\boldsymbol{E}$ and $\boldsymbol{H}$ are the amplitude and direction of the electric and magnetic fields respectively and $\boldsymbol{k}$ is the wavevector.

We Fourier transform Maxwell equations to the wavevector and frequency space, where the differential operators may be replaced by products with $\nabla \to i\boldsymbol{k}$ and $\partial/\partial t \to -i\omega$. We obtain

$$\boldsymbol{k} \times \boldsymbol{E} = \frac{\omega}{c}\boldsymbol{B}, \qquad \boldsymbol{k} \times \boldsymbol{H} = -\frac{\omega}{c}\boldsymbol{D}. \tag{B.34}$$

Applying the curl to Faraday's law given in Eq. 2.1c, we obtain

$$\boldsymbol{k} \times (\boldsymbol{k} \times \boldsymbol{E}) = \frac{\omega}{c}(\boldsymbol{k} \times \boldsymbol{H}) = -\left(\frac{\omega}{c}\right)^2 \boldsymbol{D}. \tag{B.35}$$

Expanding the double cross product, $\boldsymbol{k} \times (\boldsymbol{k} \times \boldsymbol{E}) = \boldsymbol{k}\boldsymbol{k} \cdot \boldsymbol{E} - k^2\boldsymbol{E}$. The same equation can be written as

$$\left[\boldsymbol{k}(\boldsymbol{k} \cdot \boldsymbol{E}) - k^2\boldsymbol{E} + \left(\frac{\omega}{c}\right)^2 \boldsymbol{\epsilon} \cdot \boldsymbol{E}\right] = 0. \tag{B.36}$$

This is an eigenequation whose non-trivial solutions (for non-zero electric fields) exist if the characteristic equation,

$$\det\left(\boldsymbol{k} \times (\boldsymbol{k} \times \mathbf{1}) + \left(\frac{\omega}{c}\right)^2 \boldsymbol{\epsilon}\right) = 0, \tag{B.37}$$

is satisfied. Eq. (B.37) leads to the *dispersion relation*, namely, the relation between the wavevector $\boldsymbol{k}$ and the frequency ω. Then, using the Eq. (B.36) we can obtain the directions of the electric field vector associated to these propagations.

In isotropic media, where $\boldsymbol{\epsilon} = \epsilon$ is a scalar, the double vector product in Eq. (B.36) is simplified to

$$\boldsymbol{k} \times (\boldsymbol{k} \times \boldsymbol{E}) = \boldsymbol{k}\boldsymbol{k} \cdot \boldsymbol{E} - k^2\boldsymbol{E} = -k^2\boldsymbol{E}, \tag{B.38}$$

since from Gauss equation we have $\boldsymbol{\nabla} \cdot \boldsymbol{D} = 0 \to \boldsymbol{k} \cdot \epsilon\boldsymbol{E} = \epsilon\boldsymbol{k} \cdot \boldsymbol{E} = 0$. Then the equation of propagation is reduced to

$$\left[k^2 - \left(\frac{\omega}{c}\right)^2 \epsilon\right] \cdot \boldsymbol{E} = 0. \tag{B.39}$$

Defining the dispersion relation as

$$k^2 = \left(\frac{\omega}{c}\right)^2 \epsilon. \tag{B.40}$$

Now let us consider a uniaxial anisotropic medium, where two out of the three diagonal components of the dielectric tensor are equal. Physically this means that there's a preferential direction, along an *optical axis*, also known as the extraordinary axis, ortogonal to an isotropic plane. The plane normal to the optical axis contains the ordinary direction, because of the form of the dispersion relation along each direction. To study the eigenmodes and the dispersion relations, it is most convenient to work in the coordinate system defined by the optical axis and the wavevector $\boldsymbol{k}$ of the wave we are studying. Arbitrarily, we choose the $\hat{\boldsymbol{z}}$ direction as the extraordinary axis. The dielectric tensor is expressed then as

$$\boldsymbol{\epsilon} = \begin{pmatrix} \epsilon_t & 0 & 0 \\ 0 & \epsilon_t & 0 \\ 0 & 0 & \epsilon_z \end{pmatrix}, \tag{B.41}$$

where ϵ_t is the value of components of permittivity transverse to the optical axis.

Arbitrarily we choose the $\hat{z}$ cartesian axis as the optical axis. The other two axes will be the projection of the wavevector $\boldsymbol{k}$ along the transversal plane to $\hat{z}$, given as $\boldsymbol{k}_t = \boldsymbol{k} - (\hat{z} \cdot \boldsymbol{k})\,\hat{z}$ and the orthogonal vector to $\hat{z}$ and $\hat{k_t}$, given by $\hat{z} \times \hat{k_t}$.

In this coordinate system the electric field is written as, $\boldsymbol{E} = \boldsymbol{E}_t + \boldsymbol{E}_\times + \boldsymbol{E}_z$, the sum of its projections. Rewriting the wavevector in this coordinate system, it has the form $\boldsymbol{k} = \boldsymbol{k}_t + k_z\hat{z}$, and we have $\boldsymbol{k} \cdot \boldsymbol{E} = k_t E_t + k_z E_z$ and $k^2 = k_t^2 + k_z^2$. The wave equation given in Eq. (B.36) projected

along directions $\hat{k_t}$, $\hat{z}$, and $(\hat{z} \times \hat{k_t})$ becomes three scalar equations which we write in matrix form to compute the determinant,

$$\begin{vmatrix} -k_z^2 + \left(\frac{\omega}{c}\right)^2 \epsilon_t & 0 & k_z k_t \\ 0 & -k^2 + \left(\frac{\omega}{c}\right)^2 \epsilon_t & 0 \\ k_t k_z & 0 & -k_t^2 + \left(\frac{\omega}{c}\right)^2 \epsilon_z \end{vmatrix} = 0, \tag{B.42}$$

obtaining the characteristic equation

$$(k^2 - \frac{\omega}{c}\epsilon_t)[(-k_z^2 - \frac{\omega}{c}\epsilon_t)(-k_t^2 - \frac{\omega}{c}\epsilon_z) - k_t^2 k_z^2] = 0, \tag{B.43}$$

which has two solutions

$$k_z^2 + k_t^2 = \frac{\omega}{c}\epsilon_t, \tag{B.44a}$$

$$k_z^2 \epsilon_z + k_t^2 \epsilon_t = \frac{\omega}{c}\epsilon_t \epsilon_z, \tag{B.44b}$$

corresponding to two modes of propagation. The derivation of this expresions were followed from [46].

Eq. (B.44a) has the same form as the dispersion relation of an isotropic media and corresponds to a wave polarized (with the electric field) along the perpendicular direction to both the optical axis and to its transverse plane direction. There is no effect on its propagation from the permittivity component along the optical axis direction. This mode is known as the *ordinary wave*.

The second mode of the system is described by the Eq. (B.44b) and corresponds to polarization within a plane that contains both the optical axis and its transverse plane direction. This mode is known as the *extraordinary wave* [46]. Its dispersion relation can be described by the quadratic curves

$$\frac{k_z^2}{\epsilon_t} + \frac{k_t^2}{\epsilon_z} = \left(\frac{\omega}{c}\right)^2, \tag{B.45}$$

which are ellipses when both ϵ_t and ϵ_z are positive. If any of these dielectric functions have a negative value, the dispersion curves become hyperbolas, which is why the materials that show this behaivour are called *hyperbolic materials*.

We can use the wavevector equation given by Eq. (B.45) along with the effective dielectric function given by Eq. (B.32) to obtain the impedance with Eq. (B.5) and finally obtain the surface mode with the reflection pole given by Eq. (B.11), which is a function of the width of the metal and dielectric films.

BIBLIOGRAPHY

[1] Germán Sciaini and R J Dwayne Miller. Femtosecond electron diffraction: heralding the era of atomically resolved dynamics. *Reports on Progress in Physics*, 74(9):096101, Aug 2011.

[2] Ahmed H. Zewail. 4d ultrafast electron diffraction, crystallography, and microscopy. *Annual Review of Physical Chemistry*, 57(1):65–103, 2006. PMID: 16599805.

[3] E. et al. Goulielmakis. Real-time observation of valence electron motion. *Nature.*, 466:739–743, aug 2010.

[4] Antonio Giulietti, editor. *Laser-Driven Particle Acceleration Towards Radiobiology and Medicine*. Springer Cham, 2016.

[5] Raghavan Jayakumar. *Particle Accelerators, Colliders, and the Story of High Energy Physics*. Springer Berlin, Heidelberg, 2011.

[6] Wolfgang K. H. Panofsky. *The Evolution of Particle Accelerators and Colliders*. Standford Edu, 1997.

[7] Massimo Ferrario and Bernhard J. Holzer. Introduction to particle accelerators and their limitations, 2020.

[8] T. Plettner, P. P. Lu, and R. L. Byer. Proposed few-optical cycle laser-driven particle accelerator structure. *Phys. Rev. ST Accel. Beams*, 9:111301, Nov 2006.

[9] Neil V. Sapra, Ki Youl Yang, Dries Vercruysse, J. Leedle, Dylan S. Black, R. Joel England, Su, Rahul Trivedi, Yu Miao, Olav Solgaard, L. Byer, and Jelena Vučković. On-chip integrated laser-driven particle accelerator. *Science*, 367:79–83, Jan 2020.

[10] Dongfang Zhang, Moein Fakhari, Huseyin Cankaya, Anne-Laure Calendron, Nicholas H. Matlis, and Franz X. Kärtner. Cascaded multicycle terahertz-driven ultrafast electron acceleration and manipulation. *Phys. Rev. X*, 10:011067, Mar 2020.

[11] Toshiki Tajima and John M. Dawson. Laser electron accelerator. *Physical Review Letters*, 43:267–270, 1979.

[12] A. Modena, Z. Najmudin, A. Dangor, and et al. Electron acceleration from the breaking of relativistic plasma waves. *Nature*, pages 606–608, Oct 1995.

[13] R. D'Arcy, J. Chappell, J. Beinortaite, and et al. Recovery time of a plasma-wakefield accelerator. *Nature 603*, pages 58–62, 2022.

[14] W. Horton and T. Tajima. Pump depletion in the plasma-beat-wave accelerator. *Phys. Rev. A*, 34:4110–4119, Nov 1986.

[15] Wim Leemans and Eric Esarey. Laser-driven plasma-wave electron accelerators. *Physiscs Today*, 1:44–49, 2009.

[16] F. Wu, P.A. Thomas, V.G. Kravets, and et al. Layered material platform for surface plasmon resonance biosensing. *Sci. Rep.*, pages 2045–2322, Dic 2019.

[17] S. Kawata, Y. Inouye, and P. Verma. Plasmonics for near-field nano-imaging and superlensing. *Nature Photon*, pages 388–394, Jul 2009.

[18] Nicholas Fang, Hyesog Lee, Cheng Sun, and Xiang Zhang. Sub-diffraction-limited optical imaging with a silver superlens. *Science*, 308(5721):534–537, 2005.

[19] Merlyn Jaqueline Jrz. Gtz. *Thesis: Charged Particle Intercations with Surface Plasmons.* UAEM, 2020.

[20] E. Kretschmann and H. Raether. Notizen: Radiative decay of non radiative surface plasmons excited by light. *Zeitschrift für Naturforschung A*, 23(12):2135–2136, 1968.

[21] R. H. Ritchie, E. T. Arakawa, J. J. Cowan, and R. N. Hamm. Surface-plasmon resonance effect in grating diffraction. *Phys. Rev. Lett.*, 21:1530–1533, Nov 1968.

[22] S. E. Irvine, A. Dechant, and A. Y. Elezzabi. Generation of 0.4-kev femtosecond electron pulses using impulsively excited surface plasmons. *Phys. Rev. Lett.*, 93:184801, Oct 2004.

[23] S. E. Irvine and A. Y. Elezzabi. Ponderomotive electron acceleration using surface plasmon waves excited with femtosecond laser pulses. *Applied Physics Letters*, 86(26):264102, 2005.

[24] Pochi Yeh and Amnon Yariv. Optical surface waves in periodic layered media. *Appl. Phys. Lett.*, 32:1530–1533, 1978.

[25] Ling-Bao Kong and Zhaoyang Chen. Plasmonic electron acceleration with the meta-surfaces. *Physics of Plasmas*, 24(8):083111, 2017.

[26] Jerrold Franklin. *Classical Electromagnetism.* Pearson Ed. Addison Wesley, 2005.

[27] W.L. Mochán. Plasmons. In *Reference Module in Materials Science and Materials Engineering.* Elsevier, 2016.

[28] Stefan Alexander Maier. *Plasmonics: Fundamentals and Applications.* Springer, New York, NY, 2007.

[29] N. David Mermin Neil W. Ashcroft. *Solid State Physics.* Holt, Rinehart and Winston, 1976.

[30] John David Jackson. *Classical Electrodinamics.* John Wiley, Sons, 1962.

[31] P. B. Johnson and R. W. Christy. Optical constants of the noble metals. *Phys. Rev. B*, 6:4370–4379, Dec 1972.

[32] David Pines. Collective energy losses in solids. *Rev. Mod. Phys.*, 28:184–198, Jul 1956.

[33] Pieter Kik and Mark Brongersma. *Surface Plasmon Nanophotonics*, volume 131, pages 1–9. Springer, 09 2007.

[34] C. J. Powell and J. B. Swan. Origin of the characteristic electron energy losses in aluminum. *Phys. Rev.*, 115:869–875, Aug 1959.

[35] A. Otto. Excitation of nonradiative surface plasma waves in silver by the method of frustrated total reflection. *Z. Physik*, 216:398–410, Aug 1968.

[36] E. Kretschmann and H. Raether. Notizen: Radiative decay of non radiative surface plasmons excited by light. *Zeitschrift für Naturforschung A*, 23, 12 1968.

[37] W. Barnes, A. Dereux, and T. Ebbesen. Surface plasmon subwavelength optics. *Nature*, 424:824–830, 8 2003.

[38] J. M. Gutierrez Villarreal, J. A. Gaspar Armenta, and L. A. Mayoral Astorga. Surface plasmon field enhancement: excitation by a short pulse or narrow beam of light. *J. Opt. Soc. Am. B*, 35(5):1040–1045, May 2018.

[39] Heinz Raether. *Surface Plasmons on Smooth and Rough Surfaces and on Gratings*, volume 111. Springer, 1988.

[40] Amitabh Ghoshal and Pieter G. Kik. Theory and simulation of surface plasmon excitation using resonant metal nanoparticle arrays. *Journal of Applied Physics*, 103(11):113111, 2008.

[41] H. Ditlbacher, J. R. Krenn, A. Hohenau, A. Leitner, and F. R. Aussenegg. Efficiency of local light-plasmon coupling. *Journal of Applied Physics*, 83(18):3665, 2003.

[42] Hora Heinrich. *Laser Plasma Physics: Forces and the Nonlinearity Principle*. SPIE, 2016.

[43] P. M. van den Berg. Reflection by a grating: Rayleigh methods. *J. Opt. Soc. Am.*, 71(10):1224–1229, Oct 1981.

[44] Jan Chochol and K. Postava et al. Plasmonic behavior of iii-v semiconductors in far-infrared and terahertz range. *Journal of the European Optical Society-Rapid Publications*, 2017.

[45] et al. Francisco J. Garcia-Vidal, Antonio I. Fernández-Domínguez. Spoof surface plasmon photonics. *Rev. Mod. Phys.*, 2022.

[46] Constantin Simovski and Sergei Tretyakov. *An Introduction to Metamaterials and Nanophotonics*. Cambridge University Press, 2020.